The accessibility of human centromeric chromatin is modulated by elastic CENP-A nucleosomes

Daniël P. Melters[1,a], Mary Pitman[1,2,a], Tatini Rakshit[1,a], Minh Bui[1,b], Emilios K. Dimitriadis[3,b], Garegin A. Papoian[2,#], and Yamini Dalal[1,#]

1 National Cancer Institute, Center for Cancer Research,

Laboratory of Receptor Biology and Gene Expression, Bethesda, MD

2 University of Maryland, Department of Chemistry and Biochemistry, College Park, MD

3 National Institute of Biomedical Imaging and Bioengineering, Bethesda, MD

a: Contributed equally

b: Contributed equally

Corresponding authors: dalaly@mail.nih.gov and gpapoian@umd.edu

Summary

Histone variants fine-tune transcription, replication, DNA damage repair, and faithful chromosome segregation. The histone H3 variant CENP-A/CENH3 seeds the kinetochore, creating the physical interface between centromeric chromatin and mitotic spindles. How kinetochore proteins modify CENP-A nucleosome dynamics and how these dynamics affect centromere chromatin is poorly understood. Using interdisciplinary analyses, we report that CENP-A nucleosomes are intrinsically more elastic than H3 nucleosomes, and that the kinetochore component CENP-C suppresses this innate elasticity. Shifting the balance between elastic and stiffer CENP-A states *in vivo* results in the suppression of centromeric chromatin plasticity, so that centromeric chromatin becomes less permissive to RNA polymerase 2, thereby

diminishing new CENP-A loading, ensuing in mitotic defects. Restoring this balance rescues mitotic defects. Together, these data provide a link between innate structural properties possessed by histone variant nucleosomes, the adaptability of chromatin states *in vivo*, and the epigenetic plasticity of the underlying locus.

Introduction

The adaptive nature of chromatin states allows a cell to replicate, divide, differentiate, regulate transcription, and repair damaged DNA[1,2]. In part, this dynamic chromatin landscape is shaped by removing old and incorporating new nucleosomes with and without specific histone variants[3-5], and by incorporating covalent modifications[6-8]. How different histone variants convey unique biophysical properties of their nucleosomes to the chromatin fiber, and whether non-canonical nucleosomes modulate chromatin dynamics is a subject of intense study.

One of the most striking cellular events is mitosis, when chromosomes condense into rod-shaped structures, temporarily yet dramatically changing the transcriptional landscape[9,10]. Once properly aligned at the metaphase plate, chromosomes are segregated. This is a crucial mechanical process, where chromosomes are actively pulled from the metaphase plate towards the poles[11]. This process relies, in part, on the presence of specialized centromeric nucleosomes. Epigenetically the centromere is marked by the enrichment of the histone H3 variant CENP-A/CENH3[12-16]. Despite lack of sequence conservation at the level of CENP-A or its associated DNA[12,17] in most species, centromeric chromatin recruits a triad of foundational inner kinetochore proteins: CENP-B, CENP-C, and CENP-N[18-21]. Deleting either CENP-A or CENP-C results in cell death or induces senescence after a few cell cycles[22,23]. This lag in cell death suggests that CENP-A and CENP-C are present in excess over that required to form a functional

kinetochore for one cell cycle. The additional long-lived nature of CENP-A and CENP-C guarantees faithful chromosome segregation even after their genes have been deleted[24-28]. However, for new CENP-A to be incorporated by its chaperone HJURP, centromeres must be transcribed in late mitosis/early G1[27,29,30]. A major paradox is that active transcription normally requires accessible chromatin. How this is accomplished at a time when kinetochore-bound centromeric chromatin is engaged in completion of mitosis remains a fundamental question. Consequently, elucidating biophysical features of the inner kinetochore-associated chromatin, composed of CENP-A nucleosomes and its closest bound partners such as CENP-C, is of paramount interest.

To investigate these questions, in this report, we used *in silico*, *in vitro*, and *in vivo* tools to dissect the dynamic nature of CENP-A nucleosomes compared to H3 nucleosomes, either with, or without CENP-C. Using all-atom molecular dynamic simulations, we found that CENP-A nucleosomes are highly distortable compared to H3 nucleosomes, but CENP-C fixes specific conformational states of CENP-A nucleosomes. We computationally and experimentally test the global changes of nucleosome dynamics and relative effective elasticity of free CENP-A nucleosomes in comparison to bound configurations. To our surprise, both *in silico* and *in vitro* methods show that CENP-A is far more elastic relative to H3 nucleosomes. Remarkably, upon CENP-C binding *in vitro*, CENP-A nucleosomes markedly stiffen by three-fold, and cause three-dimensional clustering of either recombinant, or native CENP-A chromatin fibers. In parallel, we demonstrate that overexpression of CENP-C *in vivo* leads to overcompaction of centromeric chromatin, which we show is concomitant with a marked reduction in the levels of RNA polymerase 2 (RNAP2) occupancy at centromeres, and with reduced *de novo* CENP-A loading in early G1. Finally, we show that overexpressing CENP-C leads to extensive mitotic defects,

which can be rescued by expressing mutants of CENP-A which are either unable to bind CENP-C, or which cause CENP-C to be sequestered away. Together, these data suggest a model in which the innate structural properties of histone variant nucleosomes regulate the plasticity and fidelity of human centromeres *in vivo*.

Results

In silico CENP-A nucleosomes are intrinsically elastic, and are suppressed by CENP-C^{CD}

In previous computational work, we reported that CENP-A nucleosomes are conformationally more distortable than H3 nucleosomes[31]. We were curious to assess precisely how CENP-C, which is CENP-A's closest binding partner, influences its nucleosomal dynamics. Here, using all-atom molecular dynamics, we first measured CENP-A nucleosome stiffness and examined spontaneous structural distortions that occur in the presence of CENP-C. We ran three simulations for this study: (1) the CENP-A nucleosome core particle (NCP), (2) the CENP-A NCP with one bound CENP-C^{CD}, and (3) the CENP-A NCP with two copies of CENP-C^{CD}. As a control, we compared these systems to canonical H3 nucleosomes[31].

Using all-atom details, we first probed conformational changes induced by CENP-C^{CD} in the context of previous experimental results[32,33]. Our modeling shows a drop in histone motions relative to each other upon binding of CENP-C^{CD}, consistent with experiments which have reported that CENP-A histones become more compact when bound to CENP-C[32] (Figure S1A). (Specific histone residue fluctuation changes are discussed in the Supplemental section for each system, Figure S1B). Next, we assessed DNA gyre sliding and gaping by labeling the same nucleic acids as in previous sm-FRET experiments[33]. We discovered that a single CENP-C^{CD} fragment dampens CENP-A nucleosome gyre gaping and DNA slides asymmetrically away from

the CENP-C bound-face of CENP-A nucleosomes. In contrast, two CENP-C^{CD} fragments freeze both, gaping and sliding motions in accordance with experimental data (Figure S1C,D, Supplemental Movie)[33].

Using these simulations, we next developed a new analysis technique in order to predict a discrete physical property, namely the elasticity of nucleosomes *in silico*. Briefly, this technique makes simplified geometric arguments to derive the Young's modulus from equilibrium simulations (Methods). We modeled the nucleosomes as homogenous elastic cylinders and calculated the dimensions and fluctuations of the "minimal" cylinders (Figure 1A). These analyses predict that the Young's modulus of CENP-A is far more elastic (6.2 MPa) than that of H3 (9.8 MPa). Interestingly, upon binding either one CENP-C^{CD}, or two CENP-C^{CD} fragments (Figure 1B), CENP-A nucleosomes adopt a stiffer configuration closer to that of H3 (8.2 MPa and 8.7MPa, respectively).

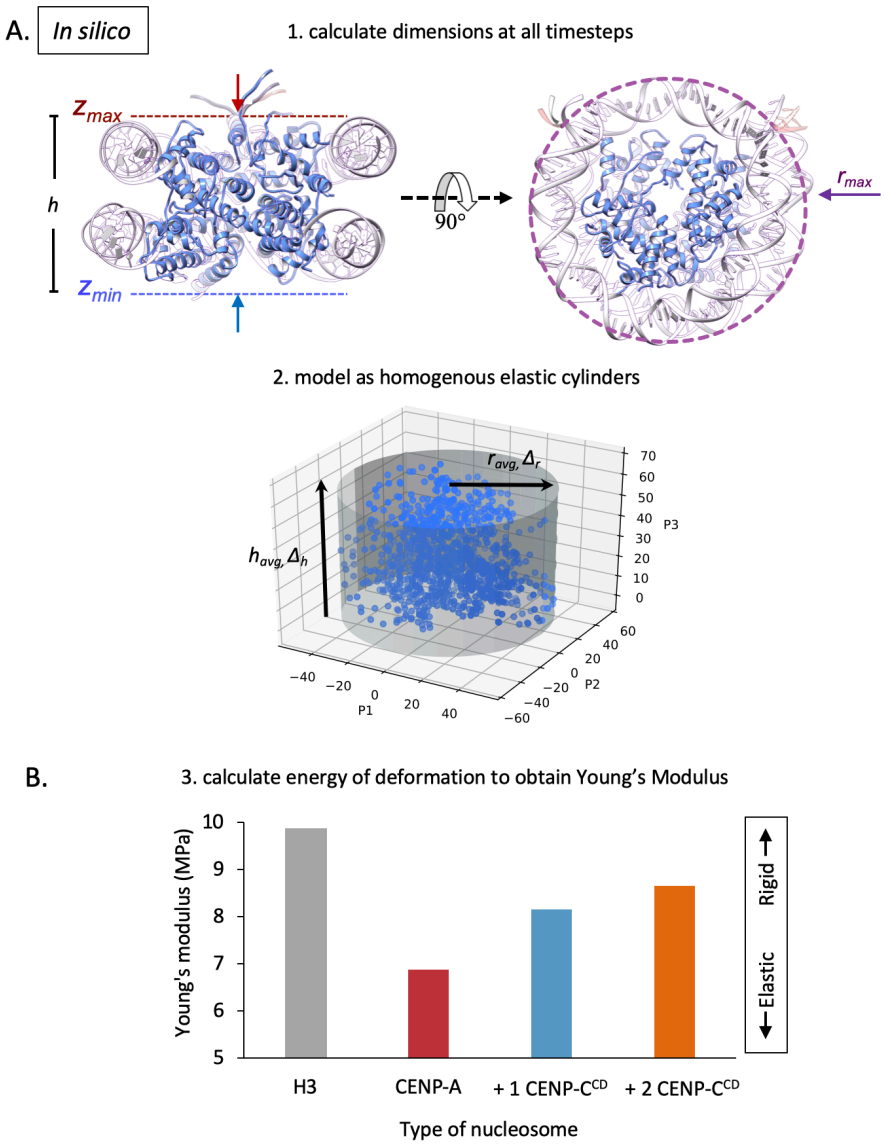

Figure 1. *In silico* analysis predicts that CENP-A nucleosomes are more elastic than H3 nucleosomes

(A) To obtain Young's modulus values from simulation, we measured the *in silico* dimensions of nucleosomes by compression of an encapsulating cylinder programmed to stop at stiffer surfaces resistant to collapse. From the heights, $h = z_{max} - z_{min}$, and the radii, r_{max}, of the resulting minimal cylinders we then calculated the average height of each system (h_{avg}), and average radius (r_{avg}). The square root of the variances of the height and radius distributions are the change in the height (Δh) and radius (Δr). (B) We then treated the nucleosomes as elastic homogenous cylinders, calculated the energy of deformation, and retrieved the Young's modulus of a cylinder vibrating at equilibrium in a thermal bath.

These data make clear predictions about a physical property, which can be measured *in vitro*. Accordingly, we turned our investigation to the next layer of complexity, *in vitro* measurements of mononucleosomes and nucleosome arrays.

In vitro CENP-A nucleosomes are highly elastic compared to H3 nucleosomes

The Young's modulus from the *in silico* experiments predict that CENP-A nucleosomes are about more elastic compared to H3 nucleosomes (Figure 1B). Therefore, we wanted to directly measure nucleosomal elasticity of mononucleosomes and nucleosomal arrays. In order to do this, we turned to nanomechanical force spectroscopy, which allows physical compression and release of particles, from which effective elasticity can be calculated. Despite the longstanding use of nanomechanical force spectroscopy[34,35], we were surprised to discover that the elasticity of nucleosomes, of any kind, has never been reported. Indeed, very few nano-indentation experiments of single protein or protein complexes have been performed[36-44]. Therefore, we developed a protocol to perform in-fluid, single-molecule, nano-indentation force spectroscopy of nucleosomes (Methods).

We set out to determine the relative elasticity (Young's modulus) of H3 and CENP-A mononucleosomes and nucleosomal arrays under physiological conditions. We reconstituted H3 and CENP-A mononucleosome arrays either on linear fragments (Figure S2), or on plasmids (Figure 2A). First, we determined in-fluid nucleosomal dimensions of H3 and CENP-A nucleosomes. Consistent with previous work[45,46], we found that *in vitro* reconstituted CENP-A nucleosomes possess dimensions similar to H3 nucleosomes (3.8±0.3 and 3.7±0.3 nm, resp.) (Table 1, Figure S3, Table S1).

Next, using mononucleosomes and a metric to deduce orientation (Methods), we established that vast majority of nucleosomes lay flat on mica (Figure S2). While CENP-A and H3 mononucleosomes are generally uniformly elastic across their surface (Figure S2), CENP-A nucleosomes are more elastic compared to H3 nucleosome by a factor of 2 (Table 1, Figure S2).

Nucleosomes exist in arrays *in vivo*. To this end, we extended our in-fluid nano-indentation force spectroscopy approach to arrays of CENP-A and H3 nucleosomes reconstituted under identical conditions and on identical plasmids (Methods). Indeed, consistent with our computational results (Figure 1B), and with the result for mononucleosomes (Figure S2), the effective Young's moduli of H3 and CENP-A nucleosomes were remarkably distinct. H3 nucleosomes possessed a Young's modulus of 11.3±4.5 MPa, whereas CENP-A nucleosomes were nearly twice as elastic at 5.8±3.9 MPa (Figure 2B, Table 1, Figure S4).

Nucleosome	N	FC	Young's Modulus (MPa)	Height (nm)	Diameter (nm)	Volume (nm^3)
Mononucleosomes						
H3	5	24	35.4±13.9	5.2±0.53	11.3±1.2	371±107
CENP-A	4	34	18.5±15.6	5.7±0.53	11.7±2.3	387±86
Nucleosome arrays						
H3	48	997	11.3±4.1	3.8±0.3	14.0±1.2	393±68
CENP-A	46	977	5.8±3.0	3.7±0.3	13.7±1.0	370±61
+ 2X CENP-C^{CD}	48	1000	9.4±5.8	4.1±0.5	13.5±0.9	394±61
+ 4X CENP-C^{CD}	50	1014	15.2±10.5	4.1±0.6	14.0±1.2	426±61

Table 1. Nanomechanical force spectroscopy indicates that CENP-C^{CD} stiffens and suppresses innate CENP-A nucleosomal elasticity. Either H3 or CENP-A nucleosomes were *in vitro* reconstituted on plasmid DNA and imaged in fluid in the presence or absence of 2-fold or 4-fold excess CENP-C^{CD}. Values were rounded up to 1 decimal point. N = number of nucleosomal particles measured. FC = number of force curves measured. For each condition, at least three independent replicates were performed (Nucleosomal Dimensions in Table S1; Elasticity raw data in Supplemental Data File 1).

In vitro CENP-C^{CD} stiffens CENP-A nucleosomes

Our *in silico* experiments (Figure 1) predict that CENP-C^{CD} alters CENP-A nucleosomal elasticity. We also tested this notion *in vitro*. First, we measured the dimensions of CENP-A:CENP-C^{CD} nucleosomes, finding that relative to free CENP-A nucleosomes (3.7±0.3 nm), when bound to CENP-C, CENP-A nucleosomes increase slightly in height (4.1±0.4 nm), (Table 1, Figure S3,Table S1). Next, we measured Young's moduli of bound vs. free CENP-A nucleosomes under the same conditions (Methods).

With the addition of 2-fold excess CENP-C^{CD}, we observed that while half the CENP-A nucleosomes remained highly elastic (~5 MPa), whereas the other half lost elasticity by a factor of three (~14.5 MPa) (1-way ANOVA $P<0.0001$; Figure 2B, Table 1, Figure S4). We interpreted this bimodal distribution to mean the CENP-A+CENP-C^{CD} population most likely represents two distinct CENP-A sub-species: one free (~5 MPa), and the other bound to CENP-C^{CD} (~14.5 MPa). To test this idea, we doubled the amount of CENP-C^{CD} to 4-fold excess over the number of CENP-A nucleosomes. Under these conditions, virtually all CENP-A nucleosomes become stiffer (15.2±10.6 MPa, Figure 2B, Table 1, Figure S4).

Therefore, *in silico,* and *in vitro* CENP-A nucleosomes possess innate elasticity, whereas CENP-C^{CD} strongly suppresses the freedom of motions of CENP-A nucleosomes. These modeling and nano-indentation data suggest that CENP-C fixes the elastic CENP-A nucleosome into a less distortable, and potentially, less open form.

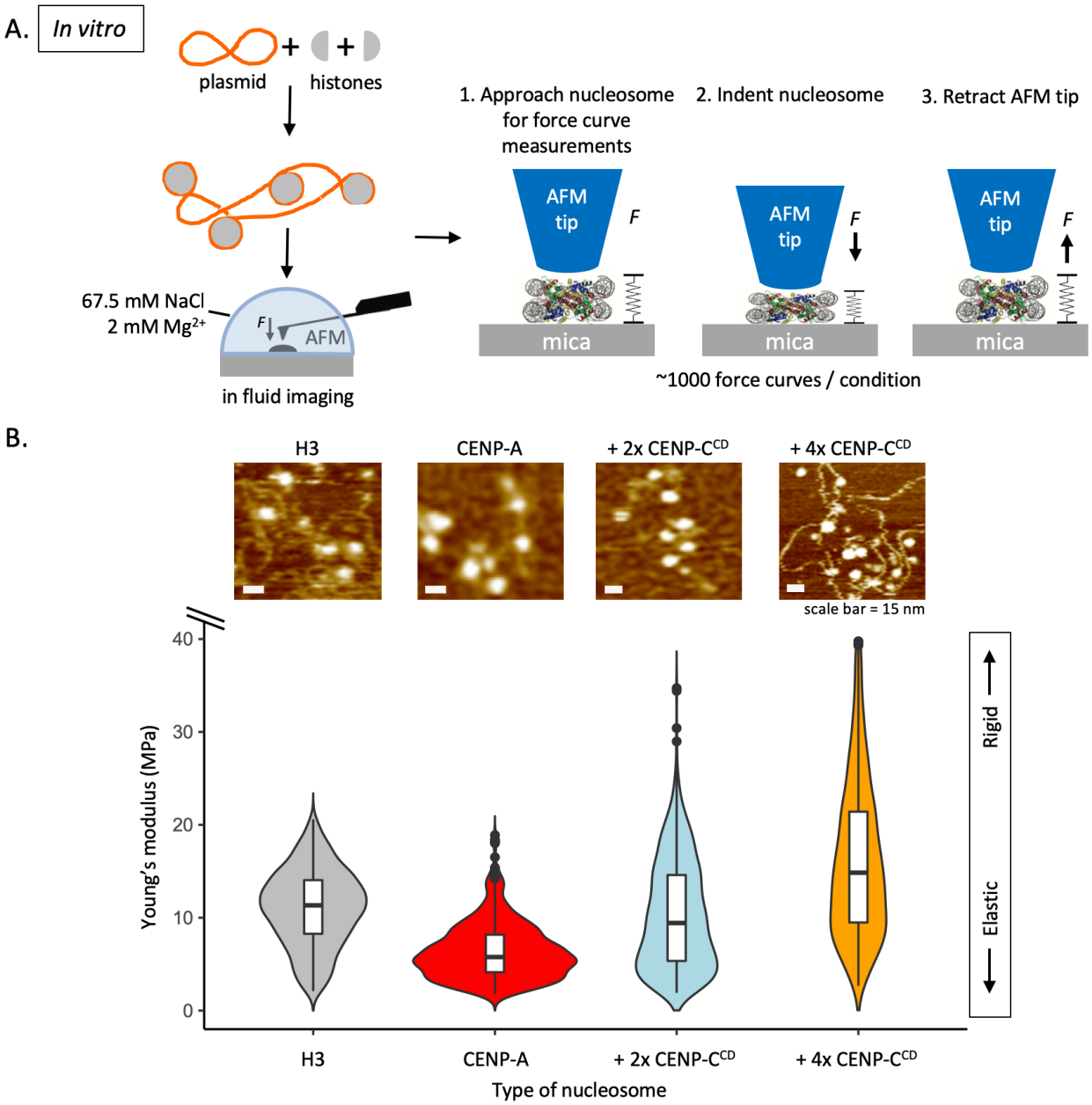

Figure 2. ***In vitro*** **CENP-C^{CD} binding stiffens elastic CENP-A nucleosomes**

(A) To determine the Young's modulus of CENP-A and H3 nucleosome arrays, we *in vitro* reconstituted H3 and CENP-A nucleosome arrays by salt dialysis, followed by nano-indentation force spectroscopy. (B) Violin plot with box plot summarizing the Young's modulus values showing that CENP-A nucleosomes are more elastic than H3 nucleosomes but become stiffer upon addition of CENP-C^{CD} (ANOVA test $P<0.0001$). Outliers for CENP-A + 4x CENP-C^{CD} were excluded from this graph. ~1000 force curves were measured per condition.

Altering the balance between elastic and stiffer CENP-A domains changes chromatin accessibility

We were very interested to elucidate potential functions for a balance between elastic vs. stiffened CENP-A nucleosomes *in vivo.* Our data above (Figure 1,2) suggests that free CENP-A nucleosomes intrinsically possess higher entropy and elasticity relative to H3. Intuitively, it might require more energy to contain such chromatin into confined three-dimensional spaces, thereby inherently possessing an unsuppressable chromatin state. By extension of our *in silico* and *in vitro* analyses (Figures 1,2), in which CENP-C suppresses innate elasticity of individual CENP-A nucleosomes in an array, we were curious whether it might also suppress an open CENP-A chromatin state into a more closed state.

We first sought to tease out this idea by incubating *in vitro* reconstituted CENP-A chromatin arrays with or without CENP-C^{CD}, and observed these arrays by AFM under standardized conditions (Methods). We noticed that upon addition of CENP-C^{CD}, *in vitro* reconstituted CENP-A arrays demonstrated a quantitative increase in clustering (Figure S5). This clustering was not observed for critical controls, namely CENP-C incubated with either H3 chromatin, or naked DNA (Figure S5). We were curious whether *ex-vivo*, CENP-A chromatin could be induced to cluster simply by the addition of the recombinant CENP-C^{CD} fragment to kinetochore-depleted CENP-A chromatin purified from human cells (Figure 3). We incubated purified kinetochore-depleted CENP-A chromatin with the recombinant CENP-C^{CD} fragment, and again measured clustering using AFM imaging. Relative to free CENP-A chromatin, we observed a ~1.2-fold increase in chromatin clusters upon CENP-C^{CD} incubation (34±6% vs 42±4%, two-sided t-test 0.015, Figure 3B, S6B, Table S2).

A logical prediction from these results is that excess CENP-C might likewise induce a more compacted chromatin state *in vivo*. To test this idea, we overexpressed full-length CENP-C *in vivo* in human cells for three days, after which we purified kinetochore-depleted CENP-A chromatin by serial N-ChIP (Figure 3A). Again, we quantified native CENP-A chromatin clusters using the same method as above (Figure 3A, Methods). Upon full-length CENP-C overexpression, we observed a ~1.7-fold increase in number of chromatin clusters relative to wild-type control (37±10% vs 64±11%, two-sided t-test 0.004, Figure 3C, S6C, Table S2). Thus, *in vitro*, *ex vivo*, and *in vivo*, addition of CENP-C shifts the balance between the population of open CENP-A chromatin vs. more closed clusters.

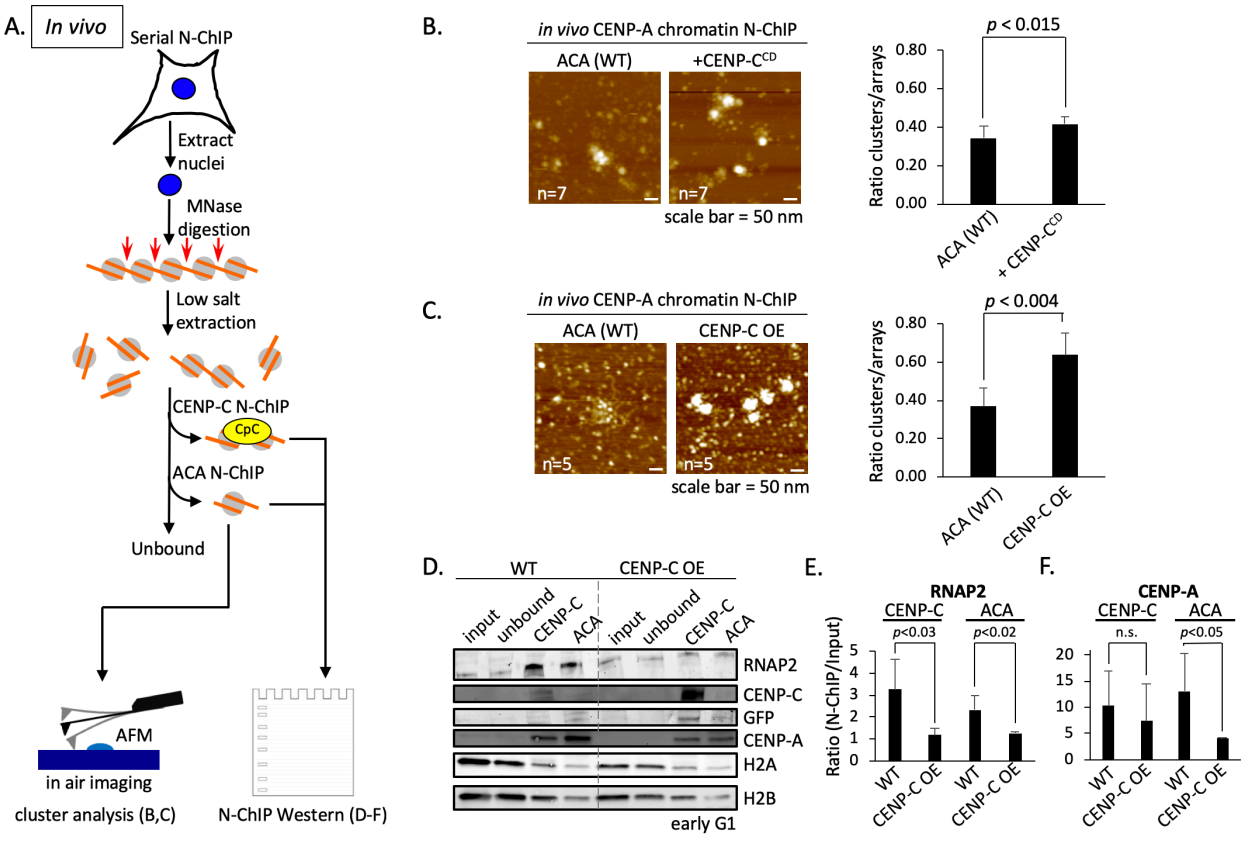

Figure 3. CENP-C overexpression compacts CENP-A chromatin, making it inaccessible to RNAP2

(A) Graphical representation of serial N-ChIP experimental procedure. For chromatin cluster analysis, the ACA N-ChIP sample was subjected to atomic force microscopy analysis, whereas SDS-page Western blot analysis focused

on both N-ChIP samples. (B) To determine if the CENP-C^{CD} fragment used in the *in vitro* experiments could induce CENP-C chromatin compaction, we added CENP-C^{CD} for 30 minutes to isolated free CENP-A chromatin from HeLa cells. Compacted chromatin was scored over the total number of nucleosome arrays. (C) Similar analysis were performed on unbound CENP-A chromatin extracted from cells that either did (CENP-C OE) or did not (WT) overexpress CENP-C. (D) Western blot of serial N-ChIP probing for RNAP2 and various centromere and chromatin markers. Quantification of (E) RNAP2 and (F) CENP-A levels were determined by LiCor's software. The bar graphs represent three independent experiments.

CENP-C overexpression suppresses centromeric RNA polymerase 2 occupancy

It is widely acknowledged that chromatin accessibility is strongly prognostic of transcriptional competency across the genome[47,48]. This correlation was first reported decades ago in landmark papers which demonstrated nuclease hypersensitivity of actively transcribing loci[49,50]. We hypothesized that a more accessible CENP-A chromatin state might likewise be permissive of transcription. In accordance with our findings above, CENP-C suppresses CENP-A elasticity (Figures 1-2), and clusters centromeric chromatin (Figure 3). *In vivo*, we hypothesized, excess CENP-C would likewise reduce centromeric chromatin accessibility, which would be reflected in reduced occupancy of transcriptional machinery.

To examine this issue, we overexpressed full length CENP-C for three days and synchronized the cells to early G1. We purified CENP-C bound centromeric chromatin as well as any residual CENP-A chromatin by serial N-ChIP. As above, we analyzed chromatin clustering of purified arrays from either wildtype, or CENP-C overexpressed cells, finding a significant increase in CENP-A chromatin clusters under the latter condition (Figure 3C).

Next, we assessed occupancy of active RNAP2 on these purified native chromatin arrays. By western blot analysis, we observed a significant reduction in RNAP2 levels on centromeric

chromatin (3- and 2-fold reduction, resp.; two-sided t-test $p<0.05$; Figure 3D,E, Table S3). Thus, CENP-C overexpression leads to both, CENP-A chromatin clustering, and reduction in RNAP2 occupancy.

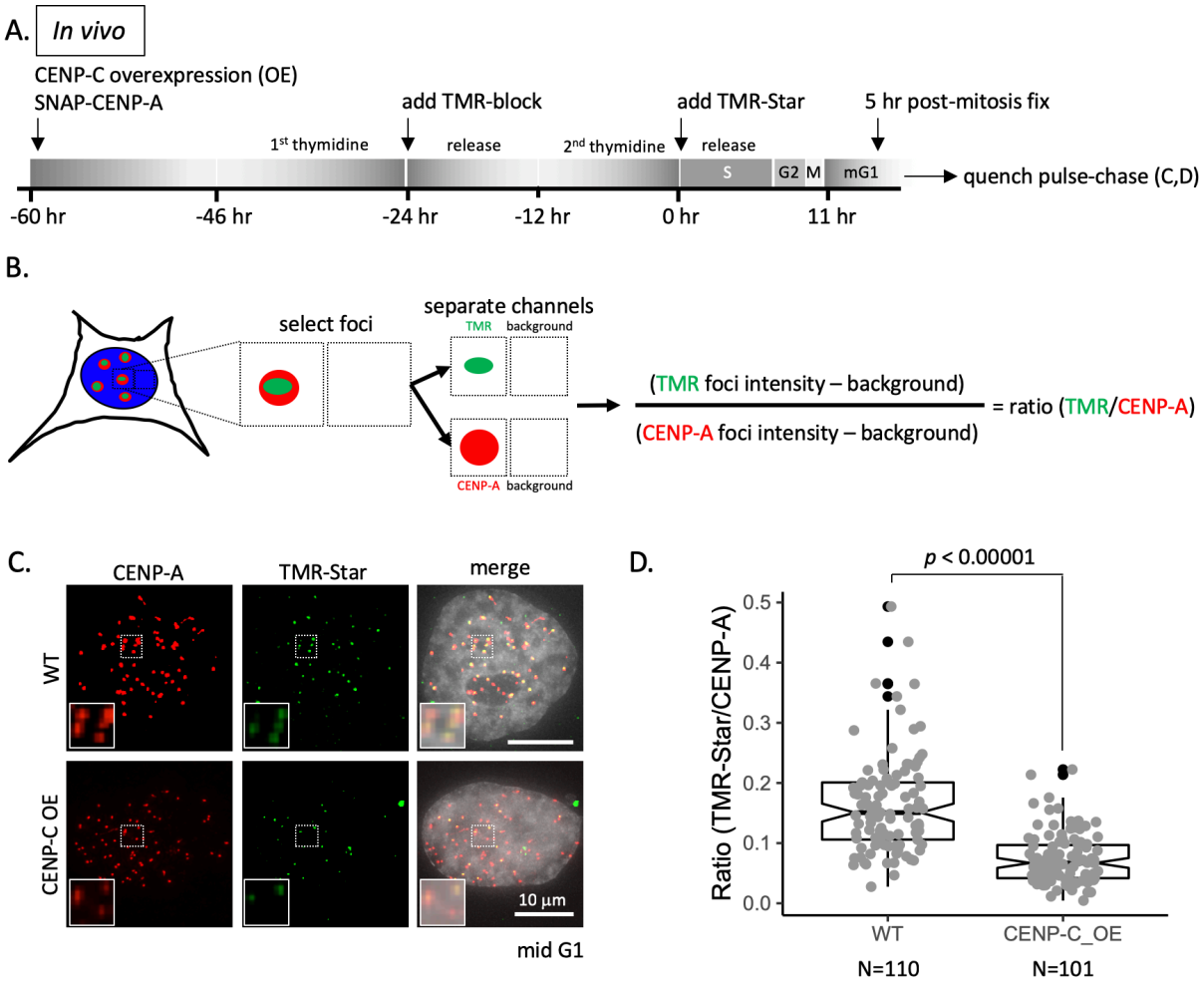

Figure 4. New CENP-A loading impaired upon CENP-C overexpression

(A) Schematic of experimental design. (B) Colocalizing immunofluorescent signal for CENP-A and TMR-Star are collected and the intensity of both foci is measured as well as background directly neighboring the foci to determine the ratio TMR-star signal over total CENP-A signal. (C) *De novo* CENP-A incorporation was assessed by quench pulse-chase immunofluorescence. After old CENP-A was quenched with TMR-block, newly loaded CENP-A was stained with TMR-Star and foci intensity was measured over total CENP-A foci intensity. Inset is a 2x

magnification of the dotted box in each respective image. (D) Quantification of *de novo* CENP-A loading by measuring the ratio of TMR-Star signal over total CENP-A signal (also in Table S4; Supplemental Raw Data File 2).

CENP-C overexpression limits *de novo* CENP-A loading

RNAP2 mediated centromeric transcription has been shown to be critical for *de novo* CENP-A loading[51]. A logical extension of our findings, is that limiting access of the transcriptional machinery to CENP-A chromatin (Figure 3C-D) should reduce new CENP-A loading. An initial clue supporting this possibility was deduced from our initial western blot analysis, in which overexpression of CENP-C led to a significant reduction in the free CENP-A population (two-sided t-test $p<0.05$; Figure 3F, Table S3). To test whether CENP-C overexpression would specifically lead to a reduction in new CENP-A loading, we turned to the well-established SNAP-tagged CENP-A system combined with quench pulse-chase immunofluorescence[27]. Using this system in cells synchronized to mid-G1, one can distinguish between older CENP-A (TMR-block) and newly incorporated CENP-A (TMR-Star) (Figure 4A,B). Strikingly, in the CENP-C overexpression background, in which we observed RNAP2 is depleted from centromeric chromatin in early G1 (Figure 3D,E), we concomitantly observed a 2.3-fold reduction of *de novo* incorporation of CENP-A (two-sided t-test $p<0.01$; Figure 4C,D; Table S4; Supplemental Raw Data File 2). Therefore, *in vivo* CENP-C overexpression leads to loss of CENP-A chromatin accessibility (Figure 3B,C), suppression of RNAP2 occupancy (Figure 3D,E), and a reduction in *de novo* CENP-A loading (Figure 4C,D).

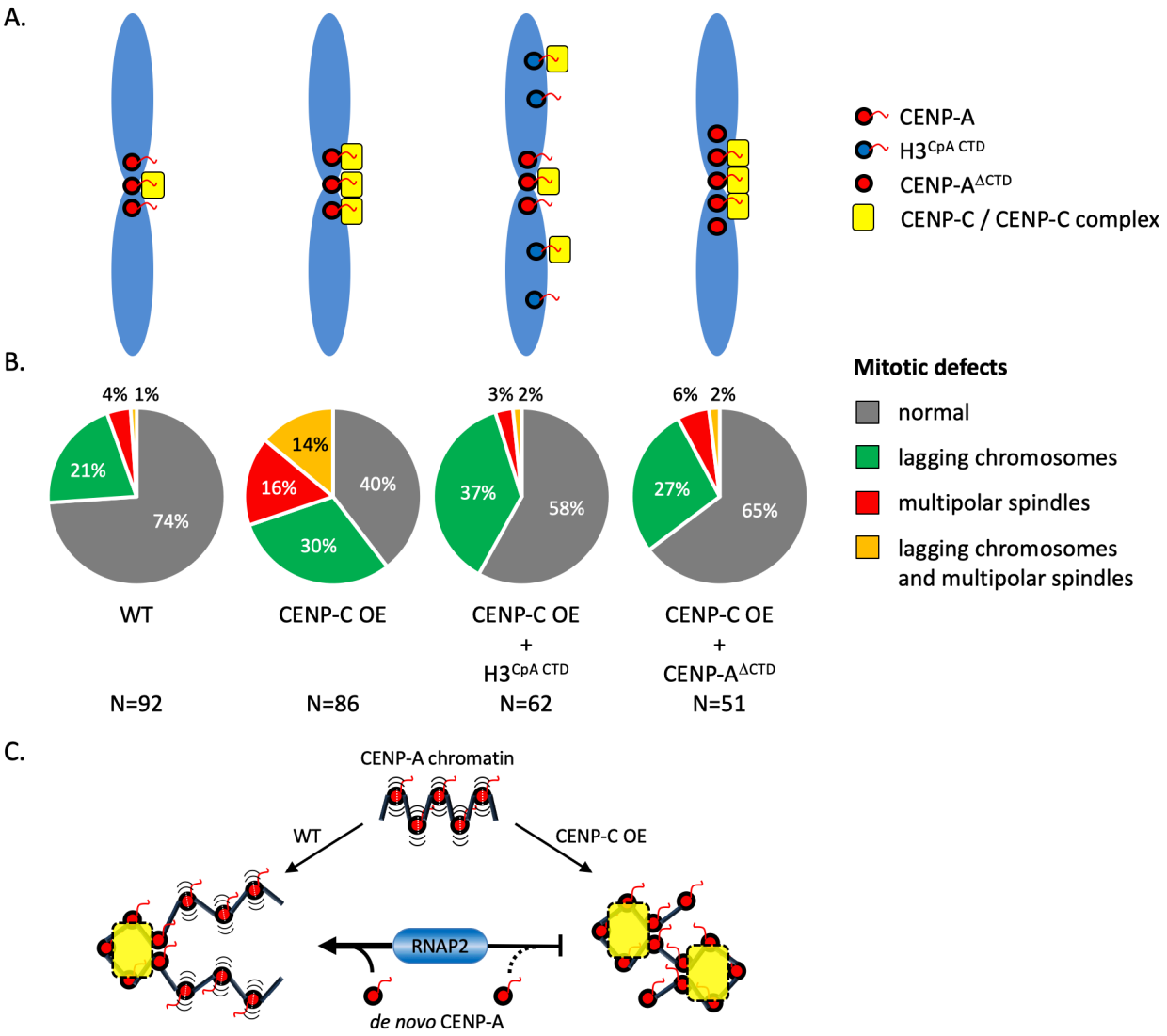

Figure 5. CENP-C overexpression leads to increased mitotic defects, which can be rescued with CENP-A CTD mutants

(A) Three days of ectoptic overexpression of CENP-C, which were synchronized to M phase, resulted in dramatic increase in mitotic defects compared to wild-type cells. The C-terminal tail of CENP-A is essential for recruitment of CENP-C. We reasoned that to rescue the mitotic deffect of CENP-C overexpression by co-expressing histone H3 with the C-terminal tail of CENP-A ($H3^{CpA\ CTD}$) or CENP-A lacking its C-terminal tail ($CENP\text{-}A^{\Delta CTD}$). (B) Mitotic defects were quantified. We observed that the level of both multipolar spindle (red) and multipolar spindle with lagging chromosome (orange) were reduced to wild-type levels. (C) Working mode: the elastic CENP-A chromatin creates an intrinsic open chromatin state that is permissive of the recruitment of the transcriptional machinery, which in turn is critical for *de novo* incorporation of CENP-A. In addition, a subset of the available CENP-A nucleosomes

will bind to the kinetochore through CENP-C. These bound CENP-A nucleosomes will stiffen and allow CENP-A chromatin to compact. When this balance is disturbed by for instance CENP-C overexpression, CENP-A chromatin becomes overcompacted, which impedes the necessary recruitment of the transcriptional machinery, and subsequently reduced new CENP-A loading.

CENP-A mutants rescue mitotic defects caused by CENP-C overexpression

As has been reported previously in chicken DT-40 cells[22], we observed that overexpressing CENP-C resulted in a quantifiable increase in mitotic defects (40% normal, 60% abnormal) relative to wildtype cells (74% normal, 26% abnormal), most notably lagging chromosomes and multipolar spindles (Figure 5A,B). However, we did not see an appreciable increase in centromere chromatin breaks as detected by gamma-H2A.X staining during mitosis, suggesting the defects are perhaps not driven by increased kinetochore:spindle attachment in the CENP-C overexpression background (Figure S6).

CENP-C functionally docks at C-terminal tail of CENP-A nucleosomes[19,33,34,52,53]. We reasoned that expressing CENP-A mutants which can either sequester away excess CENP-C, or which are insensitive to CENP-C, should rescue the defects noted above. Therefore, in the background of CENP-C over-expression, we expressed either a fusion of H3 with the C-terminal tail of CENP-A ($H3^{CpA\ CTD}$) which can bind CENP-C, or CENP-A lacking its C-terminal tail ($CENP\text{-}A^{\Delta CTD}$) which can still be deposited to centromeres by the chaperone HJURP, but which cannot bind CENP-C (Figure 5A).

In the background of CENP-C overexpression, $H3^{CpA\ CTD}$ should function as a sink for excess CENP-C. In contrast, $CENP\text{-}A^{\Delta CTD}$ should reintroduce a free CENP-A population. Indeed, upon scoring mitotic cells in the background of overexpressing CENP-C and the two mutants, we

observed that multipolar spindle defects were rescued by both $H3^{CpA\ CTD}$ (58% normal, 42% abnormal), or CENP-$A^{\Delta CTD}$ (65% normal, 35% abnormal) (Figure 5B).

Together, these data suggest that in the CENP-C overexpression background, there is enhanced CENP-A clustering (Figure 3C), depletion of RNAP2 at the centromeric chromatin (Figure 3D,E), reduced incorporation of *de novo* CENP-A (Figure 4C,D), and an increase in mitotic defects (Figure 5B). Reintroducing either a free CENP-A population or $H3^{CpA\ CTD}$ sink results in a rescue of mitotic defects. Together, these data supporting a model where a balance between bound and free CENP-A chromatin is important for proper centromere integrity.

Discussion

Not all nucleosomes are identical, as many contain histone variants, giving them distinct structures and functions[3-5]. In this report, using *in silico*, *in vitro* and *in vivo* approaches, we systematically tease apart how a single histone variant encodes intrinsic biophysical properties to its nucleosome, which can be modified by its cognate protein partner, thereby impacting both, the structural, and functional, state of the resulting chromatin fiber. Using novel *in silico* computational modeling and *in vitro* single molecule nano-indentation force spectroscopy, we directly measured effective elasticity of nucleosomes and found that CENP-A nucleosomes possess higher effective elasticity relative to canonical nucleosomes (Figure 1,2). Our finding of noticeably elastic CENP-A nucleosomes has important thermodynamic and structural implications. Specifically, one expects from general statistical physics reasoning that CENP-A nucleosomes contain excess entropy compared to canonical nucleosomes, which, in turn, will be lost upon formation of compacted chromatin. Hence, one may anticipate extra entropic resistance to compaction for chromatin enriched with CENP-A nucleosomes.

CENP-C is the essential CENP-A binding protein, which facilitates the assembly of the kinetochore[54,55], and has been shown to alter local CENP-A nucleosomes dynamics[32,33,53]. Previous FRET and hydrogen/deuterium exchange mass spectrometry experiments focused on how local CENP-A mononucleosome dynamics were altered upon CENP-C^{CD} binding. These data suggested that CENP-C^{CD} could restrict DNA gyre gapping and/or sliding, as well as increase protection of the internal H4/H2A interface[32,33,53]. Combined with our previous computational modeling where we showed that CENP-A can capture multiple conformational states[31], we predicted that CENP-C^{CD} might fix one or a few conformational states of the CENP-A nucleosome. Indeed, when we modeled CENP-A nucleosomes alone, vs. those bound to CENP-C^{CD}, we observed marked diminution of nucleosome motions, and increased Young's moduli, representing lost conformational flexibility (Figure 1B, S1). Direct elasticity measurements by nano-indentation force spectroscopy confirmed that CENP-C^{CD} increased the CENP-A Young's modulus (Figure 2B).

Are free CENP-A nucleosomes are simply a placeholder for additional CENP-C binding or might they serve another function? In this report, we observe that overexpression of CENP-C resulted in centromere chromatin clustering, Intrigingly, we note that the chromatin clustering phenotype of CENP-C is strongly reminiscent of the role of linker histone H1 in canonical chromatin compaction[56], which is important because CENP-A nucleosomes are insensitive to H1 because of their short αN-helix, which prevents the DNA entry/exit strands from crossing[57]. In addition, CENP-C overexpression decreased localization of RNAP2 at centromeric chromatin, which results in loss of *de novo* CENP-A loading (Figure 3, 4), ensuing in mitotic defects (Figure

5B). Finally, these defects can be rescued by expressing mutants that either sequester away excess CENP-C or which introduce additional free CENP-A chromatin (Figure 5A,B).

These results lend themselves to a working model in which free CENP-A nucleosomes contribute to the accessibility of the centromeric chromatin fiber, in part based on their intrinsic elasticity, and in part, because these nucleosomes may deform and slide more easily. In contrast, CENP-C stiffens CENP-A nucleosomes, limiting its capacity to deform, locking one configuration into place, thereby permitting chromatin compaction. In our working model, a balance between kinetochore bound stiffer CENP-A nucleosomes, and free elastic CENP-A nucleosomes must exist to maintain the fidelity of centromere chromatin. Indeed, the intrinsically open chromatin state provided by free CENP-A nucleosomes could also result in recruitment of other factors, including Mis18BP1[58] and and the transcriptional machinery[51]. This in turn facilitates incorporation of new CENP-A nucleosomes; an essential step required to maintain the epigenetic fidelity of centromeric chromatin (Figure 5C). When this balance is disturbed, it results in the loss of free CENP-A chromatin, for instance through overexpression of CENP-C, the level of centromeric CENP-A will reduce, jeopardizing centromeric fidelity. This working model, we think, also sheds light on the paradox of how centromeric transcription required for new CENP-A loading is enabled in the context of actively engaged kinetochores.

We note that centromeric DNA and centromeric protein genes are rapidly evolving[12-17,59]. Not all species share all kinetochore components: centromeric genes are lost, duplicated, and sometimes invented[60-62]. Despite these evolutionary changes, the distinctive chromatin structure of centromeres must be maintained, to accomplish its conserved function during mitosis. Investigating whether CENP-A structures and their elasticities are conserved, or co-evolve with

specific kinetochore proteins, will provide critical clues into what drives the evolution of centromeres, in turn serving as an excellent model for studying the evolution of epigenetic systems in the genome.

Authors contribution

Conceptualization: DPM, MP, GAP, and YD; Methodology: DPM, TR, MP, MB, EKD, GAP, and YD; Investigation: DPM, TR, MP, MB, and EKD; Writing: DPM, MP, GAP, and YD.; Funding Acquisition: EKD, GAP, and YD; Visualization: DPM, MP, and EKD; Supervision: GAP, and YD.

Acknowledgements

We thank Tom Misteli, Sam John, and members of our laboratory for critical comments; Will Heinz and Emilios Dimitriadis for discussions on force spectroscopy experiments; Carlos S Floyd for independent validation of *in silico* Young's modulus calculations; Stephan Diekmann, Dan Foltz, and Lars Jansen for gifting GFP-CENP-C and SNAP-tagged CENP-A constructs, respectively. DPM, TR, MB, EKD, and YD are supported by the Intramural Research Program of the National Institutes of Health. MP is supported by the joint NCI-UMD Cancer Technology Partnership. GAP is supported by NSF grant CHE-1363081.

References

1. Peterson, C.L. & Almouzni, G., 2013, Nucleosome dynamics as modular systems that integrate DNA damage and repair, *Cold Spring Harb Perspect Biol*, 5(9), pp. a012658.
2. Yadav, T., Quivy, J.P., & Almounzi, G., 2018, Chromatin plasticity: a versatile landscape that underlies cell fate and identity, *Science*, 361(6409:, pp. 1332-6.

3. Bellush, J.M., & Whitehouse, I., 2017, DNA replication through a chromatin environment, *Philos Trans R Soc Lond B Biol Sci*, 372(1731), pp. 20160287
4. Petryk, N., Dalby, M., Wenger, A., Stromme, C.B., Strandsby, A., Andersson, R., & Groth, A., 2018, MCM2 promoters symmetric inheritance of modified histones during DNA replication. *Science*, 361(6409), pp. 1388-92.
5. Weber, C.M., & Henikoff, S., 2014, Histone variants: dynamic punctuation in transcription, *Genes Dev*, 28(7), pp. 672-82.
6. Rothbart, S.B., & Strahl, B.D., 2009, Interpreting the language of histone and DNA modifications. *Biochim Biophys Acta*, 1839(8), pp. 627-43.
7. Luger, K., Dechassa, M.L., & Tremethick, D.J., 2012, New insights into nucleosome and chromatin structure: an ordered state or a disordered affair? *Nat Rev Mol Cell Biol*, 13(7), pp. 436-47.
8. Bowman, G.D. & Poirier, M.G., 2015, Post-translational modifications of histones that influence nucleosome dynamics, *Chem Rev*, 115(6), pp. 2274-95.
9. Palozola, K.C., Liu, H., Nicetto, D., & Zaret, K.S., 2018, Low-level, global transcription during mitosis and dynamic gene reactivation during mitotic exit, *Cold Spring Harb Symp Quant Biol*, 82, pp. 197-205.
10. Ginno, P.A., Burger, L., Seebacher, J., Iesmantavicius, V., & Schübeler, D., 2018, Cell cycle-resolved chromatin proteomics reveals the extent of mitotic preservation of the genomic regulatory landscape. *Nat Commun*, 9(1), pp. 4048.
11. Bloom, K.S., 2008, Beyond the code: the mechanical properties of DNA as they relate to mitosis, *Chromosoma*, 117(2):103-10.
12. Cooper, J.L. & Henikoff, S., 2004, Adaptive evolution of the histone fold domain in centromeric histones, *Mol Biol Evol*, 21(9), pp. 1712-8.

13. Malik, H.S. & Henikoff, S., 2001, Adaptive evolution of Cid, a centromere-specific histone in Drosophila, *Genetics*, 157(3), pp. 1293-8.
14. Talbert, P.B., Bryson, T.D. & Henikoff, S., 2004, Adaptive evolution of centromere proteins in plants and animals, *J Biol*, 3(4), p. 18.
15. Meraldi, P., McAinsh, A.D., Rheinbay, E. & Sorger, P.K., 2006, Phylogenetic and structural analysis of centromeric DNA and kinetochore proteins, *Genome Biol*, 7(3), p. R23.
16. Maheshwari, S., Tan, E.H., West, A., Franklin, F.C., Comai, L. & Chan, S.W., 2015, Naturally occurring differences in CENH3 affect chromosome segregation in zygotic mitosis of hybrids, *PLoS Genet*, 11(1), p. e1004970.
17. Melters, D.P., Bradnam, K.R., Young, H.A., Telis, N., May, M.R., Ruby, J.G., Sebra, R., Peluso, P., Eid, J., Rank, D., et al, 2013, Comparative analysis of tandem repeats from hundreds of species reveals unique insights into centromere evolution, *Genome Biol*, 14(1), p. R10.
18. Régnier, V., Vagnarelli, P., Fukagawa, T., Zerjal, T., Burns, E., Trouche, D., Earnshaw, W. & Brown, W., 2005, CENP-A is required for accurate chromosome segregation and sustained kinetochore association of BubR1, *Mol Cell Biol*, 25(10), pp. 3967-81.
19. Carroll, C.W., Milks, K.J. & Straight, A.F., 2010, Dual recognition of CENP-A nucleosomes is required for centromere assembly, *J Cell Biol*, 189(7), pp. 1143-55.
20. Mendiburo, M.J., Padeken, J., Fülöp, S., Schepers, A. & Heun, P., 2011, Drosophila CENH3 is sufficient for centromere formation, *Science*, 334(6056), pp. 686-90.
21. Pesenti, M.E., Weir, J.R. & Musacchio, A., 2016, Progress in the structural and functional characterization of kinetochores, *Curr Opin Struct Biol*, 37, pp. 152-63.

22. Fukagawa, T., Pendon, C., Morris, J. & Brown, W., 1999, CENP-C is necessary but not sufficient to induce formation of a functional centromere, *The EMBO journal*, 18(15), pp. 4196-209.

23. McKinley, K.L. & Cheeseman, I.M., 2016, The molecular basis for centromere identity and function, *Nat Rev Mol Cell Biol*, 17(1), pp. 16-29.

24. Kalitsis, P., Fowler, K.J., Earle, E., Hill, J. & Choo, K.H., 1998, Targeted disruption of mouse centromere protein C gene leads to mitotic disarray and early embryo death, *Proc Natl Acad Sci U S A*, 95(3), pp. 1136-41.

25. Howman, E.V., Fowler, K.J., Newson, A.J., Redward, S., MacDonald, A.C., Kalitsis, P. & Choo, K.H., 2000, Early disruption of centromeric chromatin organization in centromere protein A (Cenpa) null mice, *Proc Natl Acad Sci U S A*, 97(3), pp. 1148-53.

26. Suzuki, A., Hori, T., Nishino, T., Usukura, J., Miyagi, A., Morikawa, K. & Fukagawa, T., 2011, Spindle microtubules generate tension-dependent changes in the distribution of inner kinetochore proteins, *J Cell Biol*, 193(1), pp. 125-40.

27. Bodor, D.L., Valente, L.P., Mata, J.F., Black, B.E. & Jansen, L.E., 2013, Assembly in G1 phase and long-term stability are unique intrinsic features of CENP-A nucleosomes, *Mol Biol Cell*, 24(7), pp. 923-32.

28. Smoak, E.M., Stein, P., Schultz, R.M., Lampson, M.A. & Black, B.E., 2016, Long-Term Retention of CENP-A Nucleosomes in Mammalian Oocytes Underpins Transgenerational Inheritance of Centromere Identity, *Curr Biol*, 26(8), pp. 1110-6.

29. Foltz, D.R., Jansen, L.E., Balley, A.O., Yates, Jr 3rd, J.R., Bassett, E.A., Wood, S., Black, B.E., & Cleveland, D.W., 2009, Centromere-specific assembly of CENP-A nucleosomes is mediated by HJURP. *Cell*, 137(3), pp. 472-84.

30. Dunleavy, E.M., Roche, D., Tagami, H., Lacoste, N., Ray-Gallet, D., Nakamura., Y., Daigo., Y., Nakatani, Y., & Almouzni-Pettinotti, G., 2009, HJURP is a cell-cycle-dependent maintenance and deposition factor of CENP-A at centromeres. *Cell*, 137(3), pp. 485-97.

31. Winogradoff, D., Zhao, H., Dalal, Y. & Papoian, G.A., 2015, Shearing of the CENP-A dimerization interface mediates plasticity in the octameric centromeric nucleosome, *Sci Rep*, 5, p. 17038.

32. Falk, S.J., Guo, L.Y., Sekulic, N., Smoak, E.M., Mani, T., Logsdon, G.A., Gupta, K., Jansen, L.E., Van Duyne, G.D., Vinogradov, et al, 2015, Chromosomes. CENP-C reshapes and stabilizes CENP-A nucleosomes at the centromere, *Science*, 348(6235), pp. 699-703.

33. Falk, S.J., Lee, J., Sekulic, N., Sennett, M.A., Lee, T.H. & Black, B.E., 2016, CENP-C directs a structural transition of CENP-A nucleosomes mainly through sliding of DNA gyres, *Nat Struct Mol Biol*, 23(3), pp. 204-8.

34. Heinz, W.F., & Hoh, J.H., Spatially resolved force spectroscopy of biological surfaces using the atomic force microscope. *Trends Biotechnol.* 17(4):143-50 .

35. Butt, H.-J., Cappella, B., & Kappl, M., 2005, Force measurements with the atomic force microscope: technique, interpretation and application, *Surface Sci Rep*, 59:1-152.

36. Garcia, A.E., 1992, Large-amplitude nonlinear motions in proteins, *Phys Rev Lett*, 68(17), pp. 2696-9.

37. Korostelev, A., & Noller H.F., 2007, Analysis of structural dynamics in the ribosome by TLS crystallographic refinement. *J Mol Biol*, 373(4), pp. 1058-70.

38. Radmacher, M., Fritz, M., Cleveland, J.P., Walters, D.A., & Hansma, P.K., 1994, Imaging adhesion forces and elasticity of lysozyme adsorbed on mica with the atomic force microscope, *Langmuir*, 10, pp. 3809-14.

39. Vinckier, A., & Semenza, G., 1998, Measuring elasticity of biological materials by atomic force miscroscopy. *FEBS Lett*, 430, pp. 12-6.

40. Afrin, R., Alam, M.T., & Atsushi, I., 2005, Pretranstion and progressive softening of bovine carbonic anhydrase II as probed by single molecule atomic force microscopy, *Protein Sci*, 14, pp. 1447-57.

41. Parra, A., Casero, E., Lorenzo, E., Pariente, F., & Vázquez, L., 2007, Nanomechanical properties of globular proteins: lactate oxidase, *Langmuir*, 23, pp. 2747-54.

42. Rakshit, T., Banerjee, S., Mishra, S., Mukhopadhyay, R., 2013, Nanoscale mechano-electronic behavior of a metalloprotein as a variable of metal content. *Langmuir*, 29(40):12511-9.

43. Roos, W.H., 2018, AFM nanoidentation of protein shells, expanding the approach beyond viruses. *Semin Cell Dev Biol*, 73, pp. 145-152.

44. Perrino, A.P., & Garcia, R, 2016, How soft is a single protein?: Stress-strain curve of antibody pentamers with 5 pN and 50 pN resolutions, *Nanoscale*, 8, pp. 9151-8.

45. Walkiewicz, M. P., Dimitriadis, E. K. & Dalal, Y., 2014, CENP-A octamers do not confer a reduction in nucleosome height by AFM, *Nat Struct Mol Biol,* 21, pp. 2-3

46. Athwal, R.K., Walkiewicz, M.P., Baek, S., Fu, S., Bui, M., Camps, J., Ried, T., Sung, M.H. & Dalal, Y., 2015, CENP-A nucleosomes localize to transcription factor hotspots and subtelomeric sites in human cancer cells, *Epigenetics Chromatin*, 8, p. 2.

47. Vermaak, D., Ahmad, K., & Henikoff, S., 2003, Maintenance of chromatin states: an open-and-shut case, *Curr Opin Cell Biol*, 15(3), pp. 266.74.

48. Bergel, S.L., 2007, The complex language of chromatin regulation during transcription, *Nature*, 447(7143), pp. 407-12.

49. Weintraub, H., & Groudine, M., 1976, Chromosomal subunits in active gene have an altered conformation, *Science*, 193(4256), pp. 848-56.

50. Wu, C., 1985, An exonuclease protection assay reveals heat-shock element and TATA box DNA-binding proteins in crude nuclear extracts, *Nature*, 317(6032), pp. 84-7.

51. Müller, S., & Almouzni, G., 2017, Chromatin dynamics during the cell cycle at centromeres, *Nat Rev Genet*, 18(3):192-206.

52. Kato, H., Jiang, J., Zhou, B.R., Rozendaal, M., Feng, H., Ghirlando, R., Xiao, T.S., Straight, A.F. & Bai, Y., 2013, A conserved mechanism for centromeric nucleosome recognition by centromere protein CENP-C, *Science*, 340(6136), pp. 1110-3.

53. Guo, L.Y., Allu, P.K., Zandarashvili, L., McKinley, K.L., Sekulic, N., Dawicki-McKenna, J.M., Fachinetti, D., Logsdon, G.A., Jamiolkowski, R.M., Cleveland, D.W., et al, 2017, Centromeres are maintained by fastening CENP-A to DNA and directing an arginine anchor-dependent nucleosome transition, *Nat Commun*, 8, p. 15775.

54. Przewloka, M.R., Venkei, Z., Bolanos-Garcia, V.M., Debski, J., Dadlez, M., & Glover, D.M., 2011, CENP-C is a structural platform for kinetochore assembly. *Curr Biol*, 21(5), pp. 399-405.

55. Klare, K., Weir, J.R., Basilico, F., Zimniak, T., Massimiliano, L., Ludwigs, N., Herzog, F., & Musacchio, A., 2015, CENP-C is a blueprint for constitutive centromere-associated network assembly within human kinetochores, *J Cell Biol*, 210(1), pp. 11-22.

56. Clausell, J., Happel, N., Hale, T.K., Doenecke, D., & Beato, M., Histone H1 subtypes differentially modulate chromatin condensation without preventing ATP-dependent remodeling by SWI/SNF or NURF, *PLoS ONE*, 4(10), e0007243

57. Roulland, Y., Ouararhni, K., Naidenov, M., Ramos, L., Shuaib, M., Syed, S.H., Lone, I.N., Boopathi, R., Fontaine, E., Papai, G., et al, 2016, The Flexible Ends of CENP-A Nucleosome Are Required for Mitotic Fidelity, *Mol Cell*, 63(4), pp. 674-85.

58. Nardi, I.K., Zasadzińska, E., Stellfox, M.E., Knippler, C.M., & Foltz, D.R., 2016, Licensing of centromeric chromatin assembly trhough the Mis18α-Mis18β heterotetramer, *Mol Cell*, 61(5), pp. 774-87.

59. Henikoff, S., Ahmad, K. & Malik, H.S., 2001, The centromere paradox: stable inheritance with rapidly evolving DNA, *Science*, 293(5532), pp. 1098-102.

60. Ross, B.D., Rosin, L., Thomae, A.W., Hiatt, M.A., Vermaak, D., de la Cruz, A.F., Imhof, A., Mellone, B.G. & Malik, H.S., 2013, Stepwise evolution of essential centromere function in a Drosophila neogene, *Science*, 340(6137), pp. 1211-4.

61. Drinnenberg, I.A., Henikoff, S. & Malik, H.S., 2016, Evolutionary Turnover of Kinetochore Proteins: A Ship of Theseus? *Trends Cell Biol*, 26(7), pp. 498-510.

62. van Hooff, J.J., Tromer, E., van Wijk, L.M., Snel, B. & Kops, G.J., 2017, Evolutionary dynamics of the kinetochore network in eukaryotes as revealed by comparative genomics, *EMBO Rep*.

Supplemental Figures S1-S7
Figure S1 – Two CENP-C^{CD} fragment strengthens stiffening of CENP-A nucleosomes
Figure S2 – Mononucleosomes lay flat and are uniformly elastic
Figure S3 – CENP-C^{CD} modestly increases CENP-A nucleosome heights
Figure S4 – Examples of force curve measurements
Figure S5 – *In vitro* reconstituted CENP-A chromatin clustered by CENP-C^{CD}, but not H3 chromatin or naked DNA.
Figure S6 – CENP-C overexpression did not increase mitotic double strand DNA breaks

Supplemental Tables S1-S4:
Table S1 – Quantification of nucleosome dimensions in H3, CENP-A, and CENP-A + CENP-C^{CD} particles.
Table S2 – Quantification of CENP-A chromatin clusters induced by CENP-C^{CD}, and in CENP-C over-expression conditions
Table S3 – Quantification of RNAP2 depletion under CENP-C over-expression conditions.
Table S4: Quantification of de novo CENP-A loading in TMR-Star experiments
Supplemental Movie – Motions of three highlighted residues on a CENP-A nucleosome.

Raw Data Files S1,S2:
Raw Data File S1 – Quantification of Young's Modulus of nucleosomes particles for H3, CENP-A, and CENP-A + 2-fold excesses CENP-C^{CD,} CENP-A + 4-fold excess CENP-C^{CD} conditions. Values are in MPa.
Raw Data File S2 – Quantification of de novo CENP-A loading by measuring foci intensity of ratio of (total CENP-A over background) and (TMR-Star over background) for WT or CENP-C overexpressed cells. Values are arbitrary units from ImageJ.

Online Methods

Key Resources Table

Antibody	Source	Identifier	Application	Quantity
ACA serum	BBI Solutions	SG140-2	N-ChIP	5 µL
α-GFP	Santa Cruz	sc-9996	WB	1:1000
α-CENP-A (mouse)	Abcam	ab13939	IF	1:1000
α-CENP-A (rabbit)	Milipore	04-205	WB	1:3000
α-CENP-C (guinea pig)	MBL International	PD030	N-ChIP	5 µL
α-CENP-C (rabbit)	Santa Cruz	sc-22789	IF, WB	1:1000; 1:500
α-RNA polymerase II	Abcam	ab5095	WB	1:500
α-γH2A.X	Abcam	ab11174	IF	1:1000
α-H2A	Abcam	ab18255	WB	1:1000
α-H2B	Abcam	ab1790	WB	1:1000

IF = immunofluorescence; N-ChIP: native chromatin immunoprecipitation, WB = western blot

Software and Algorithms	
Gwyddion	http://gwyddion.net/
Nanoscope	http://www.nanophys.kth.se/nanophys/facilities/nfl/afm/icon/bruker-help/Content/SoftwareGuide/NanoScope815CoverPage.htm
Asylum Research	Version 15
Igor Pro	https://www.wavemetrics.com/taxonomy/term/87
R	https://www.r-project.org/
ggplot2	https://ggplot2.tidyverse.org/
LiCor Image Studio	https://www.licor.com/bio/products/software/image_studio_lite/

NIH ImageJ	https://imagej.nih.gov/ij/
GraphPad Prism 8	https://www.graphpad.com/
Bio-Formats	https://www.openmicroscopy.org/bio-formats/
PyMOL	https://pymol.org/2/
CRaQ	http://facilities.igc.gulbenkian.pt/microscopy/microscopy-macros.php

Contact for Reagent and Resource Sharing

Requests for further information or reagents should be directed to the Lead Contacts: Yamini Dalal (dalaly@mail.nih.gov) and Garyk Papoian (gpapoian@umd.edu).

Experimental Model and Subject Detail

HeLa cells (female cells derived from cervical adenocarcinoma) were obtained from ATCC CCL-2 and grown at 37ºC and 5% CO2 in T-175 tissue culture flasks from Sarstedt (Cat. #83.3912.002).

Methods Details

All-atom computational modeling

We built three nucleosomal systems for simulation: the CENP-A nucleosome as described previously[1] and the CENP-A nucleosome with one and two CENP-C central domain fragment bound from PDB ID: 4X23[2]. The CENP-C^{CD} fragments were docked onto the CENP-A interface using the CE algorithm[3] of PyMOL (The PyMol Molecular Graphics System). We set up both systems to initiate from the final time point of our previous 2 μs simulation and the coordinates, velocities, parameters, and system setup and analysis methods were replicated[1]. Both CENP-A and CENP-A with one and two CENP-C^{CD} bound[2] ran for an additional microsecond and the first 600 ns of simulation time were truncated from the dataset for further analysis and to account for equilibration. For a control to compare to this dataset, we also analyzed the H3 nucleosome from our previous work[4].

Furthermore, we calculated the relative positions of three phosphate backbone atoms at positions -33, -43, and +38 numbered from the 5' (−) to 3' (+) direction relative to the pseudo-dyad. The distances between these points and the skew of the triangle formed were measured and then plotted with the initial position of residue -33 set to (0,0) on a xy-plane. The distribution of Δy and Δx of +38 relative to -33 and -34 was used to measure DNA gaping and sliding respectively. We visualized these distributions with standard box plots showing the mean, the interquartile range, and whiskers extending to the extrema. The distribution of polygons contains the minima and maxima of all three vertices were plotted visually with triangles to present changes in skew and the range of sizes. We executed RMSF and center-of-mass motion calculations as described previously[1].

In silico calculation of Young's Modulus

The goal of this analysis is to model each nucleosome as a homogenous elastic "minimal" cylinder for each time step of the simulation, retrieve the cylinder height and radius distributions, and from this data calculate the in silico Young's Modulus of the nucleosomes.

Our method to calculate the dimensions of the minimal cylinders follows the workflow:

[1] Orient the nucleosomes so that they lie "flat" on the x-y plane. To achieve this, we calculated the principal axes of the moment of inertia, where the first principal axis defines the broadest plane of the nucleosome. The axes of symmetry of the nucleosomes align with the three principal axes, p_1, p_2, p_3, with the center-of-mass at the origin.

[2] Calculate the surfaces of the cylinder so that they coincide with stiffer regions of the nucleosomes. We addressed this issue by calculating the root mean square fluctuations (RMSF) of each residue along the simulation since the structural disorder of a region positively correlates with local structural fluctuations. Since RMSF is a time-averaged parameter, multiple timesteps are required to calculate fluctuations of residues. As a result, we divided the simulation into windows (800 windows per simulation) and calculated the RMSF for each residue in each window.

[3] Retrieve the average heights, radii, and the variances of these distributions. To do so, we sorted the C-α coordinates by their z-axis coordinates and selected the z coordinate of the residue where ten stiffer residues below an RMSF threshold were excluded outside of the cylinder volume. From the height, h, and radius, r, data we calculated the average h and r, the variance or spread of the distributions, and the standard deviations Δr and Δh.

[4] The outputs from step [3] then served as the variable inputs to calculate the Young's Modulus of each system. The work done in the deformation of an elastic material is stored in the form of strain energy which we calculate for the deformation of the cylinder in the absence of the shear stresses. In our simulations, the amplitude of vibrations depends on the amount of energy given to the system from the temperature, or the thermal bath of the solvent. From equipartition theorem, $1/2\ k_bT$ (where k_b is the Boltzmann constant and T is temperature, 300 K) is the amount of energy attributed to the observed cylinder deformation. From the data on the average cylinder conformation, the magnitude of elastic deformation, and the energy input from the thermal bath we calculate the Young's modulus.

Single Molecule Nano-Indentation Force spectroscopy of mononucleosomes

H3 (H3 mononucleosome on 187bp of 601 sequence cat#16-2004, EpiCypher, Research Triangle Park, NC) and CENP-A mononucleosome (CENP-A/H4 cat#16-010, H2A/H2B cat#15-0311, 187bp of 601-sequence cat#18-2003, EpiCypher, Research Triangle Park, NC) samples were diluted 1:5 in 2 mM NaCl with 4 mM MgCl (pH7.5) and deposited onto freshly cleaved mica that had previously been treated with aminopropyl-silantrane (APS) as described[5-7]. Samples were incubated on mica for ~3 minutes, excess buffer was rinsed with 400 µL ultrapure, deionized water, and gently dried under an argon stream. Imaging was performed with a commercial AFM (MultiMode-8 AFM, Bruker, Billerica, MA) using silicon-nitride, oxide-sharpened probes (MSNL-E with nominal stiffness of 0.1 nN/nm, Bruker, Billerica, MA). Deposited sample was rehydrated with 10 mM HEPES (pH 7.5), 4 mM MgCl. Imaging was performed in AFM mode termed "Peak-Force, Quantitative NanoMechanics" or PF-QNM. Images were preprocessed using the instrument image analysis software (Nanoscope v8.15) and gray-scale images were exported to ImageJ analysis software (v1.52i). First nucleosomes were identified as decribed[5,6] and subsequently roundness was determined. The Young's modulus was determined by the instrument image analysis software (Nanoscope v8.15).

Optimization of single molecule nano-indentation force spectroscopy

Nucleosomes that lay flat, have a round appearance, whereas nucleosomes laying on their side would have an oval appearance. We measured the roundness of both H3 and CENP-A mononucleosomes and found that almost all nucleosomes had a round appearance (Supplemental Figure S2A).

The use of AFM nano-indentation of nucleosomes raise two more concerns. One is that the size of the probe is of the same order of magnitude as the nucleosome. Therefore, widely-used, Hertz-type models used to extract elasticity from indentation data would only provide an effective elasticity that depends on the indentation geometrical parameters such as probe size and precise point of indentation on the nucleosome. This effective elasticity would, however, be comparable between the two types of nucleosomes and their relative values would be comparable to those obtained *in-silico.* The probe sizes used did not vary significantly but we needed to address the possibility that the extracted elasticity depends strongly on the exact point of indentation. If the nucleosome is not uniformly elastic, the precise position of the AFM probe tip could be a critical factor. If the nucleosomes are uniformly elastic, slight differences in where on the nucleosome the elasticity is measured would not be a major concern. We therefore measured the Young's modulus across mononucleosomes (Supplemental Figure S2B). We found that, in general, effective elasticity did not vary significantly across nucleosomes (Supplemental Figure S2B).

Single Molecule Nano-Indentation Force spectroscopy of nucleosome arrays

In vitro reconstitution of CENP-A nucleosome arrays (CENP-A/H4 cat#16-010 and H2A/H2B cat#15-0311, EpiCypher, Research Triangle Park, NC) and H3 (H3/H4 cat#16-0008 and H2A/H2B cat#15-0311, EpiCypher Research Triangle Park, NC) on a 3kb plasmid containing a single 601 sequence (pGEM3Z-601 from Addgene #26656) were performed as previously described[5,6]. CENP-$C_{482-527}$ fragment[2] (ABI Scientific, Sterling, VA) was added in 2.2-fold or 4-fold molar excess to CENP-A nucleosomes. Imaging was performed by using standard AFM equipment (Oxford Instruments, Asylum Research's Cypher S AFM, Santa Barbara, CA). To be able to measure the Young's modulus, the reconstituted chromatin was kept in solution containing 67.5 mM NaCl and 2 mM Mg^{2+} and Olympus micro cantilevers (cat# BL-AC40TS-

C2) was used. Before each experiment, the spring constant of each cantilever was calibrated using both GetReal™ Automated Probe Calibration of Cypher S and the thermal noise method[8]. Obtained values were in the order of 0.1 N/m. As a reference to obtain the indentation values, the photodiode sensitivity was calibrated by obtaining a force curve of a freshly cleaved mica surface. All experiments were conducted at room temperature. Force-curves for ~50 nucleosomes for all three conditions were measured using both 'Pick a Point' and force-mapping mode. The maximum indentation depth was limited to ~1.5 nm and the maximum applied force was 150-200 pN. For our analyses, we used Hertz model with spherical indenter geometry for Young's Modulus measurements, $\delta = [3(1 - \nu^2)/(4ER^{1/2})]^{2/3}F^{2/3}$ (for a spherical indenter), where ν is the Poisson ratio of the sample, which is assumed to be 1/3 as in studies reported previously[9,10]; δ, F, E, and R are the indentation, force, Young's modulus of the sample and radius of the tip respectively. The radius of the tip was confirmed by SEM and found to be about 10 nm in width. Graphs were prepared using ggplot2 package for R.

AFM and cluster analysis

Imaging of CENP-C and CENP-A N-ChIP and bulk chromatin was performed as described[5,6] with the following modifications. Imaging was aquired by using standard AFM equipment (Oxford Instruments, Asylum Research's Cypher S AFM, Santa Barbara, CA) with silicon cantilevers (OTESPA or OTESPA-R3 with nominal resonances of ~300 kHz, stiffness of ~42 N/m) in noncontact tapping mode. Usually, 10 µl stock solution of 4× diluted CENP-C chromatin or 10× diluted ACA chromatin was deposited on APS-mica. APS-mica was prepared as previously described[5,6]. The samples were incubated for 10 min, gently rinsed, and dried with inert argon gas before imaging.

For the compaction study, we added 1 ng CENP-C^{CD} to purified ACA samples and incubated them for 30 minutes prior to deposition on APS-mica and subsequent imaging. To quantify the chromatin compaction, we manually counted chromatin clusters based on their size being at least twice as wide as an individual nucleosome, but with an identifiable entry and exit DNA strand, over the total number of nucleosome arrays. Similar analyses were performed with PC4[11], MeCP2[12], H1[13], H1 in combination with topoisomerase II[14], and different salt concentrations[15].

Native Chromatin-Immunoprecipitation and western blotting

Human cell line HeLa were grown in DMEM (Invitrogen/ThermoFisher Cat #11965) supplemented with 10% FBS and 1X penicillin and streptomycin cocktail. N-ChIP experiments were performed without fixation. After cells were grown to ~80% confluency, they were harvested as described here[1,10], but with a few modifications. In short, cells were harvested, washed with PBS and PBS containing 0.1% Tween 20 (Sigma-Aldrich cat #P7949). Nuclei were released with TM2 (20 mM Tris-HCl, pH 8.0; 2 mM $MgCl_2$; 0.5 mM PMSF) with 0.5% Nonidet P-40 (Sigma-Aldrich cat #74385). Afterwards, nuclei were washed with TM2 and dissolved in a total volume of 2 mL of 0.1 M TE (10 mM Tris-HCl, pH 8.0; 0.2 mM EDTA, 100 mM NaCl). Subsequently, chromatin was digested for 6 minutes with 0.25 U MNase (Sigma-Aldrich cat #N3755-500UN) and supplemented with 1.5 mM $CaCl_2$. MNase reaction was quenched with 10 mM EGTA. All centrifugations were done at 1000 rpm at 4ºC. The cell or nuclei pellet was only tapped once to facilitate braking them up. Supernatant was removed, and chromatin extracted overnight in low salt solution (0.5X PBS; 0.1 mM EGTA supplemented with a protease inhibitor cocktail (Roche cat #05056489001)). CENP-C N-ChIP chromatin bound to Protein G Sepharose beads (GE Healthcare cat #17-0618-02) were washed twice with ice cold 0.5X PBS and spun down for 1 minute at 4ºC at 800 rpm. For a serial N-ChIP, the first unbound fraction was saved

and subjected to a second N-ChIP with ACA serum, which contains antibodies against CENP-A, -B, and -C.. Western analysis was done using LiCor's Odyssey CLx scanner and Image Studio v2.0. For CENP-C overexpression we transfected HeLa cells with pEGFP-CENP-C using the Amaxa Cell Line Nucleofector Kit R (Lonza cat#VVCA-1001) per manufacturer's instructions. HeLa cells were synchronized to early G1 by double thymidine block (0.5 mM, Sigma-Aldrich cat#T9250). After the first block of 22 hours, cells were released for 12 hours, followed by a second thymidine block of 12 hours. Cells were released for approximately 11 hours, which corresponds to early G1, based on our previous reports[1,10,16].

Immunostaining of mitotic chromosomes

HeLa cells were synchronized to mitosis with double thymidine block. Primary antibodies CENP-C and CENP-A were used at dilution 1:1000. Alexa secondary (488, and 568) were used at dilution of 1:1000. Images were obtained using DeltaVision RT system fitted with a CoolSnap charged-coupled device camera and mounted on an Olympus IX70. Deconvolved IF images were processed using ImageJ. Mitotic defects (lagging chromosomes and/or multipolar spindles) were counted for 83 and 76 cells (mock, GFP-CENP-C, respectively).

Quench pulse-chase immunofluorescence

To quantify *de novo* assembled CENP-A particles, we transfected HeLa cells with SNAP-tagged CENP-A (generous gift from Dan Foltz) in combination with either empty vector or GFP-CENP-C using the Amaxa Nucleofector kit R (Lonza Bioscience, Walkersville, MD) per instructions. The quench pulse-chase experiment was performed according to Bodor et al[17]. In short, following transfection, cells were synchronized with double thymidine block. At the first release TMR-block (S9106S, New England Biolabs, Ipswich, MA) was added per manufactures

instruction and incubated for 30 min at 37ºC, followed by three washes with cell culture media. At the second release TMR-Star (S9105S, New England Biolabs, Ipswich, MA) was added per manufactures instructions and incubated for 15 min at 37ºC, followed by three washes with cell culture media. Fourteen hours after adding TMR-Star, cells were fixed with 1% paraformaldehyde in PEM (80 mM K-PIPES pH 6.8, 5 mM EGTA pH 7.0, 2 mM $MgCl_2$) for 10 min at RT. Next, cells were washed the cells three times with ice cold PEM. To extract soluble proteins, cells were incubated with 0.5% Triton-X in CSK (10 mM K-PIPES pH 6.8, 100 mM NaCl, 300 mM sucrose, 3 mM $MgCl_2$, 1 mM EGTA) for 5 min at 4ºC. The cells were rinsed with PEM and fixed for a second time with 4% PFA in PEM for 20 min at 4ºC. Next, the cells were washed three times with PEM. Cells were permeabilized with 0.5% Triton-X in PEM for 5 min at RT and subsequently washes three times with PEM. Next, the cells were incubated in blocking solution (1X PBS, 3% BSA, 5% normal goat serum) for 1 hr at 4ºC. CENP-A antibody (ab13979 1:1000) was added for 1 hr at 4ºC, followed by three washes with 1X PBS-T. Anti-mouse secondary (Alexa-488 1:1000) was added for 1hr at 4ºC, followed by three 1X PBS-T and two 1X PBS washes. Following air-drying, cells were mounted with Vectashield with DAPI (H-1200, Vector Laboratories, Burlingame, CA) and the coverslips were sealed with nail polish. Images were collected using a DeltaVision RT system fitted with a CoolSnap charged-coupled device camera and mounted on an Olympus IX70. Deconvolved IF images were processed using ImageJ. From up to 22 nuclei, colocalizing CENP-A and TMR-Star foci signal were collected, as well directly neighboring regions. Background signal intensity was deducted from corresponding CENP-A and TMR-Star signal intensity before the ratio CENP-A/TMR-Star was determined. Graphs were prepared using the ggplot2 package for R.

Quantification and Statistical Analyses

Significant differences for nucleosome height measurement from AFM analyses and significant differences for immunostaining quantification, and chromatin compaction quantification, were performed using the 2-sided t-test as described in the figure legends and main text. Significant differences for the Young's modulus of *in vitro* reconstituted H3, CENP-A, and CENP-A + CENP-C^{CD} were determined using 1-way ANOVA test using Graphpad Prism software. Significance was determined at $p < 0.05$.

References

1. Bui, M., Pitman, M., Nuccio, A., Roque, S., Donlin-Asp, P.G., Nita-Lazar, A., Papoian, G.A. & Dalal, Y., 2017, Internal modifications in the CENP-A nucleosome modulate centromeric dynamics, *Epigenetics Chromatin*, 10, p. 17.
2. Kato, H., Jiang, J., Zhou, B.R., Rozendaal, M., Feng, H., Ghirlando, R., Xiao, T.S., Straight, A.F. & Bai, Y., 2013, A conserved mechanism for centromeric nucleosome recognition by centromere protein CENP-C, *Science*, 340(6136), pp. 1110-3.
3. Shundyalov, I.N., & Bourne, P.E., 1998, Protein structure alignment by incremental combinatorial extension (CE) of the optimal path. *Protein Eng*, 11(9), pp. 739-47.
4. Winogradoff, D., Zhao, H., Dalal, Y. & Papoian, G.A., 2015, Shearing of the CENP-A dimerization interface mediates plasticity in the octameric centromeric nucleosome, *Sci Rep*, 5, p. 17038.
5. Walkiewicz, M. P., Dimitriadis, E. K. & Dalal, Y., 2014, CENP-A octamers do not confer a reduction in nucleosome height by AFM, *Nat Struct Mol Biol,* 21, pp. 2-3.

6. Dimitriadis, E.K., Weber, C., Gill, R.K., Diekmann, S., & Dalal Y., 2010, Tetrameric organization of vertebrate centromeric nucleosomes. *Proc Natl Acad Sci USA,* 107(47), pp. 20317-22.
7. Stumme-Diers, M.P., Banerjee, S., Hashemi, M., Sun, Z., & Lyubchenko, Y.L., 2018, Nanoscale dynamics of centromere nucleosomes and the critical roles of CENP-A. *Nucleic Acids Res*, 46(1), pp. 94-103.
8. Hutter, J.L., & Beckhoefer, J., 1993, Calibration of atomic-force microscope tips, *Rev Sci Instrum*, 64(7):1868-73.
9. Radmacher, M., Fitz, M., Cleveland, J.P., Walters, D.A., & Hansma, P.K., 1994, Imaging adhesion forces and elasticity of lysozyme adsorbed on mica with the atomic force microscope, *Langmuir*, 10(10):3809-14.
10. Rakshit, T., Banerjee, S., Mishra, S., Mukhopadhyay, R., 2013, Nanoscale mechano-electronic behavior of a metalloprotein as a variable of metal content. *Langmuir*, 29(40):12511-9.
11. Das, C., Hizume, K., Batta, K., Kumar, B.R., Gadad, S.S., Ganguly, S., Lorain, S., Verreault, A., Sadhale, P.P., Takeyasu, K., & Kundu, T.K., 2006, Transcriptional coactivator PC4, a chromatin-associated protein, induces chromatin condensation, *Mol Cell Biol*, 26(22), pp. 8303-15.
12. Georgel, P.T., Horowitz-Scherer, R.A., Adkins, N., Woodcock, C.L., Wade, P.A., & Hansen, J.C., 2003, Chromatin compaction by human MeCP2. Assembly of novel secondary chromatin structures in the absence of DNA methylation, *J Biol Chem*, 278(34), pp. 32181-8.

13. Clausell, J., Happel, N., Hale, T.K., Doenecke, D., & Beato, M., Histone H1 subtypes differentially modulate chromatin condensation without preventing ATP-dependent remodeling by SWI/SNF or NURF, *PLoS ONE*, 4(10), e0007243.
14. Hizume, K., Araki, S., Yoshikawa, K., & Takeyasu, K., 2007, Toposiomerase II, scaffold component, promotes chromatin compaction in vitro in a linker-histone H1-dependent manner, *Nucleic Acids Res*, 35(8), pp. 2787-99.
15. Bussiek, M., Müller, G., Waldeck, W., Diekmann, S., & Langowski, J., 2007, Organization of nucleosomal arrays reconstituted with repetitive African green monkey alpha-satellite DNA as analysed by atomic force microscopy, *Eur Biophys J*, 37(1), pp. 81-93.
16. Bui, M., Dimitriadis, E.K., Hoischen, C., An, E., Quénet, D., Giebe, S., Nita-Lazar, A., Diekmann, S. & Dalal, Y., 2012, Cell-cycle-dependent structural transitions in the human CENP-A nucleosome in vivo, *Cell*, 150(2), pp. 317-26.
17. Quénet, D., & Dalal, Y., 2014, A long non-coding RNA is required for targeting centromeric protein A to the human centromere, *eLife*, 3:e03254.
18. Bodor, D.L., Rodriguez, M.G., Moreno, N., & Jansen, L.E., 2012, Analysis of protein turnover by quantitative SNAP-based pulse-chase imaging, *Curr Protoc Cell Biol*, Chapter 8, Unit 8.

Supplementary Figures

Supplemental Figure S1

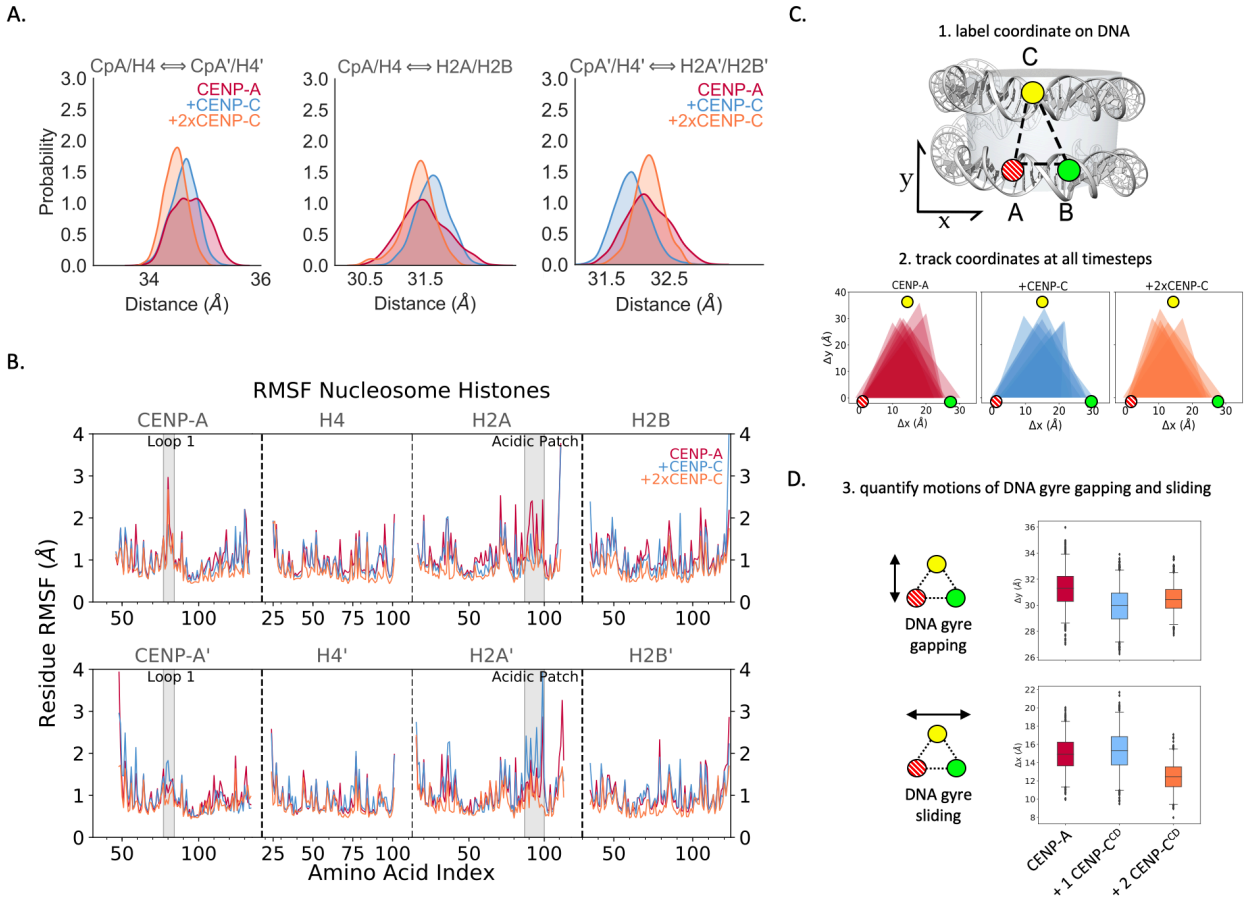

Figure S1 – Two CENP-C^{CD} fragment strengthens stifening of CENP-A nucleosomes
(A) The distance between the center of mass (COM) of histone dimers is shown in red for CENP-A, blue for CENP-A + 1 CENP-C^{CD}, and in orang for CENP-A + 2 CENP-C^{CD}. Two CENP-C^{CD} fragment exaggerated the COM distances compared to a single CENP-C^{CD} fragment, which means that 2 CENP-C^{CD} further induces a global loss of CENP-A nucleosome flexibility. (B) Residue root mean square fluctuations (RMSF) shows freezing of local flexibility in the CENP-A nucleosome shown in red, 1 CENP-C^{CD} bound shown in blue, and 2 CENP-C^{CD} bound shown in orange. In the region of CENP-C^{CD} binding, the first heterotypic half on the top panel, CENP-C is seen to freeze the acidic patch and the loop 1 region of CENP-A. One CENP-C^{CD} creates asymmetry, especially at the C-terminal end of H2A and H2B, this is abrogated when the second CENP-C^{CD} is bound. Dashed lines separate individual histones. (C) The free energy landscape of CENP-A nucleosomes alone or CENP-A nucleosome with CENP-C^{CD} fragment was determined by principle component analysis. CENP-A nucleosomes display a rugged free energy landscape, which is locked down when CENP-C^{CD} is bound, increasing the connectivity of the energetic minima. (D) All-atom computational modeling of DNA gyre gapping or DNA gyre sliding of CENP-A nucleosome alone or bound to either 1 or 2 CENP-C^{CD} fragments.

Supplemental Figure S2

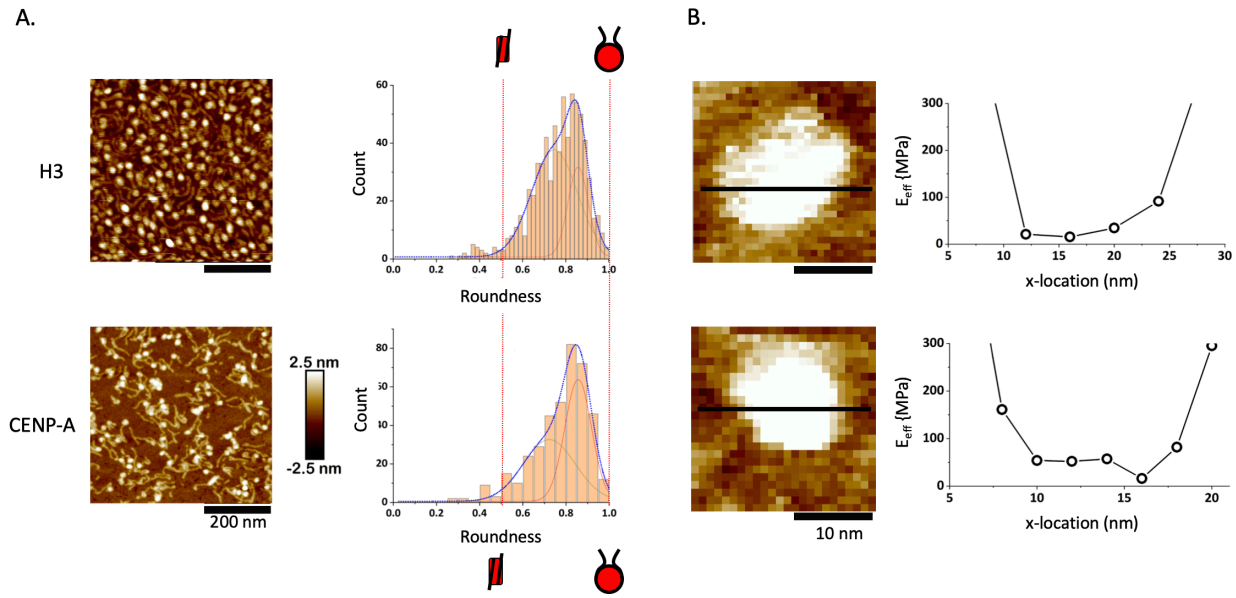

Figure S2 – Mononucleosomes lay flat and are uniformly elastic
(A) Roundness was measured of either H3 or CENP-A mononucleosomes. A value of 1 would indicate that a nucleosome particle lays flat, whereas a value of 0.5 would indicate a nucleosome particle laying on its side. Almost all nucleosomal particles lay flat on the mica surface. (B) Young's modulus was measured across either H3 or CENP-A mononucleosomes to assess whether a nucleosome particle is uniformly elastic. No significant difference was observed.

Supplemental Figure S3

A.

Predicted height	5.5 nm	5.8 nm	6.4 nm	6.6 nm
Predicted diameter	10.9 nm	10.8 nm	10.7 nm	10.6 nm

B.

Measured height	3.8±0.3 nm	3.7±0.3 nm	4.1±0.5 nm	4.1±0.6 nm
Measured diameter	14.0±1.2 nm	13.7±1.0 nm	13.5±0.9 nm	14.0±1.2 nm
Volume	589.9±106.3 nm^3	555.6±90.8 nm^3	590.8±91.2 nm^3	638±122.7 nm^3

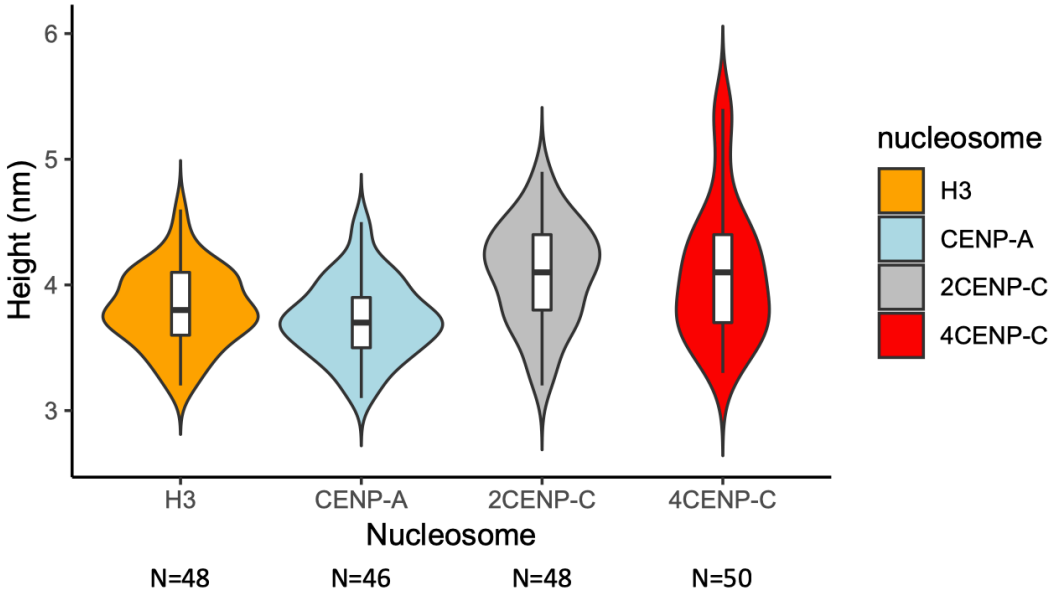

Figure S3 – CENP-C^{CD} modestly increases CENP-A nucleosome heights
(A) Height and diameter predictions from the computational modeling experiment described in Figure 1A. (B) CENP-C^{CD} modestly increases height of *in vitro* reconstituted CENP-A nucleosomes H3 and CENP-A nucleosome were in vitro reconstituted, and by in fluid AFM, we measured their dimensions (height, diameter, and volume). The height distribution is shown in the violin plot containing a bar plot. CENP-A nucleosomes are ever so slightly smaller than H3 nucleosomes. The addition of CENP-C^{CD} fragment, which can only bind CENP-A nucleosomes, we observed an increase in height and in a dose-dependent manner its volume.

Supplemental Figure S4

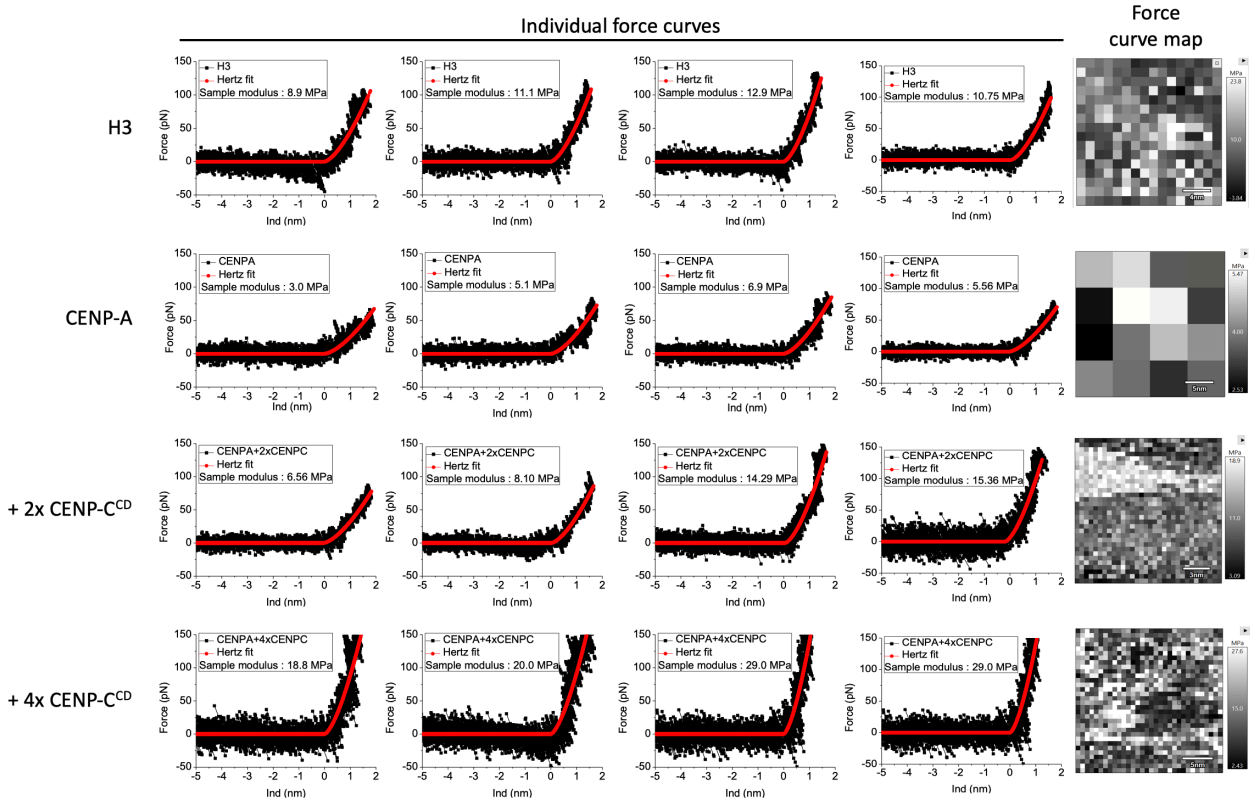

Figure S4– Examples of force curve measurements
Four representative force curves for H3 nucleosomes, CENP-A nucleosomes, CENP-A nucleosomes with 2-fold excess CENP-C^{CD} fragments, and CENP-A nucleosomes with 4-fold excess CENP-C^{CD} fragments are shown, in addition to a representative force curve map per nucleosome type.

Supplementary Figure S5

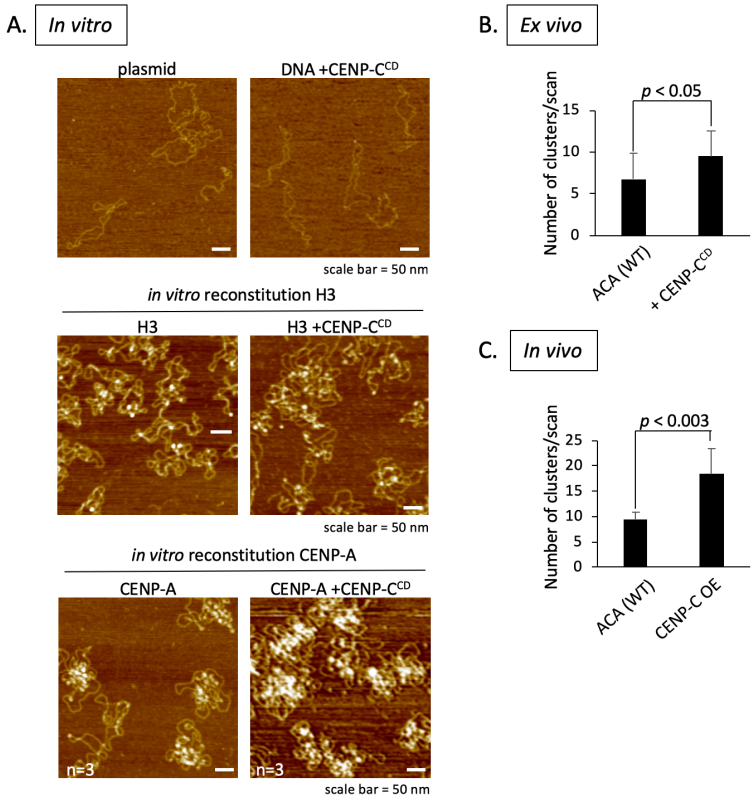

Figure S5 – *In vitro* reconstituted CENP-A chromatin clustered by CENP-C^{CD}, but not H3 chromatin or naked DNA.
(A) By in air AFM we observed that *in vitro* reconstituted CENP-A nucleosome arrays clustered in the presence of CENP-C^{CD}, but not reconstituted H3 nucleosome arrays or naked plasmid. (B) To determine if the CENP-C^{CD} fragment used in the *in vitro* experiments could induce CENP-C chromatin compaction, we added CENP-C^{CD} for 30 minutes to isolated free CENP-A chromatin from HeLa cells. Compacted chromatin was scored over the total number of nucleosome arrays. (C) Similar analysis were performed on unbound CENP-A chromatin extracted from cells that either did (CENP-C OE) or did not (WT) overexpress CENP-C.

Supplemental Figure S6

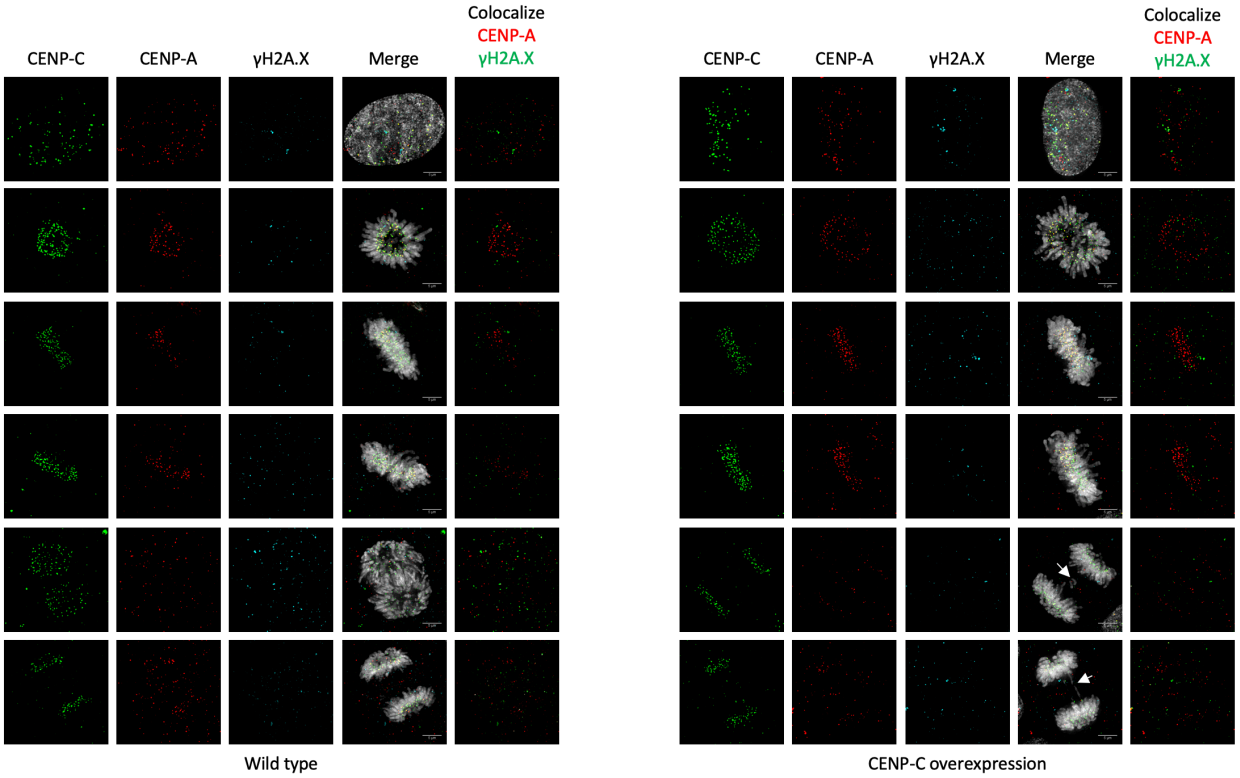

Figure S6 – CENP-C overexpression did not increase mitotic double strand DNA breaks
Representative images of either wild-type or CENP-C overexpressing HeLa cells. HeLa cells were transfected for three days and synchronize to early G1 prior to fixation and staining for CENP-C (green), CENP-A (red), γH2A.X (cyan), and DAPI (grey). No difference in number of γH2A.X foci was observed between the two samples. Arrow highlight lagging chromosomes.

Supplemental Tables 1-4

Table S1. Quantification of nucleosomal dimensions by AFM analysis. Data demonstrate that *in vitro* chromatin reconstitution yields equivalent dimensions for CENP-A and H3, but that CENP-A nucleosomes increase in height by ~0.4nm when bound to CENP-C^{CD}. Heights (nm), Diameters (nm), and volumes (nm3) were calculated for representative particles of each class of nucleosome imaged by atomic force microscopy in-fluid conditions (Methods).

Supplemental Table S1: Quantification of nucleosomal dimensions by AFM analysis												
H3			CENP-A			2X CENP-C^{CD}			4X CENP-C^{CD}		
height(nm)	diameter (nm)	volume(nm3)	height(nm)	diameter (nm)	volume(nm3)	height(nm)	diameter (nm)	volume(nm3)	height(nm)	diameter (nm)	volume(nm3)
3.8	12.3	300.8	3.7	12.8	317.2	5.4	12.5	441.5	4.7	14.1	489.1
4.1	12.3	324.6	3.7	13.4	347.6	4.5	15.1	536.9	3.6	15.1	429.5
3.2	15.1	381.8	3.1	12.5	253.4	4.4	12.8	377.2	5.4	12.8	463.1
3.5	16.7	510.8	3.2	14.4	347.2	4.3	12.8	368.6	4.4	14.2	464.4
3.7	13.5	352.8	3.2	12.6	265.8	4.3	14.1	447.3	3.7	14.8	424.1
3.9	14.3	417.3	3.5	13.9	353.8	4.3	12.7	362.9	3.6	12.5	294.3
4.2	13.5	400.5	3.5	13.5	333.8	4.2	13.4	394.6	3.6	12.7	303.7
3.9	15.5	490.3	3.6	15	423.9	4.1	14.5	451.1	3.3	15.1	393.7
3.9	14.3	417.3	3.6	13.8	358.7	4	13.1	359.2	3.8	13.6	367.8
4	12.5	327.1	3.8	14.2	400.9	3.9	13.5	371.9	4.5	15.9	595.4
3.7	15.5	465.2	3.9	14	400.1	3.8	12.8	325.8	4.1	14.7	463.5
3.7	12.7	312.3	4.1	14.1	426.5	3.8	13.6	367.8	3.8	14.1	395.6
3.7	13.5	352.8	4.5	13.6	435.5	4.8	11.9	355.7	3.7	17.5	593.1
4	12.3	316.7	4.4	12.8	377.2	4.2	13.8	418.5	3.3	15.5	414.9
3.9	14.3	417.3	4.2	12.6	348.9	4.1	13.5	391.1	5.1	15.1	608.5
4	12.5	327.1	4	12.8	342.9	3.7	14.1	384.9	4.4	16.7	642.1
3.7	15.5	465.2	4	14.6	446.2	3.4	12.8	291.5	4.4	12.5	359.7
3.3	15.5	414.9	3.9	15	459.2	3.3	15.1	393.7	4.2	13.5	400.8
3.8	14.3	406.6	3.9	13.9	394.3	3.7	13.5	352.8	4.1	14.2	432.5
4.1	14.3	438.7	3.8	13.8	378.7	3.9	12.9	339.6	3.9	12.6	324.1
3.7	15.5	465.2	3.7	14.5	407.1	4.4	12.9	383.1	3.8	13.8	378.7
4.6	15.5	578.3	3.5	12.5	286.1	3.6	13.2	328.2	3.7	14.1	384.6
4	13.1	359.2	3.4	12.8	291.5	4.1	13.6	396.8	5.6	11.9	415.1
4.4	12.7	371.3	3.3	14.2	348.2	4.2	13.9	424.6	5.4	14.3	577.8
3.4	13.9	343.7	4.1	13.6	396.8	4.2	15	494.5	4.4	13.9	444.8
3.6	12.7	303.8	4.1	14.5	451.1	4.3	13.7	422.3	4.3	13.1	386.1
4.1	13.9	414.5	4	12.5	327.1	4.6	14.9	534.4	4.2	11.9	311.2
4.1	13.1	368.2	3.8	11.9	281.6	4.7	12.3	372.1	4.1	13.1	368.2
4.3	13.9	434.7	3.8	14.9	441.5	4.9	14.1	509.8	3.9	13.9	394.3
3.8	14.3	406.6	3.8	13.2	346.5	4.5	12.7	379.8	5.4	13.2	492.4
3.6	11.9	266.7	3.7	13.6	358.1	4.5	12.8	385.8	4.5	12.3	356.2
3.8	11.9	281.6	3.7	12.8	317.2	4.5	14.2	474.8	4.1	13.2	373.8
3.6	13.1	323.3	3.7	12.9	322.2	4.4	13.2	401.2	4.1	14.5	451.1
4.1	13.9	414.5	3.7	15.6	471.2	4.1	14.2	432.6	3.9	15	459.2
3.8	13.9	384.2	4.1	15.2	495.7	4.1	13.2	373.8	3.7	14.2	390.4
4.1	15.1	489.2	3.7	12.9	322.2	3.9	14.5	429.1	3.5	13.9	353.8
4.1	14.7	463.6	3.6	13.7	353.6	3.8	12.5	310.7	3.5	14.6	390.4
3.5	12.1	268.1	3.6	13.6	348.4	3.7	12.9	322.2	3.4	14.1	353.7
3.4	13.9	343.7	3.6	16.2	494.4	3.4	14.7	384.4	3.5	13.7	343.7
3.7	14.3	395.9	3.5	14.6	390.4	3.2	12.6	265.8	3.6	14.7	407.1
3.4	15.5	427.4	3.4	12.7	286.9	3.6	12.7	303.8	3.8	12.9	330.9
4.1	13.9	414.5	3.4	15.1	405.7	3.7	14.3	395.9	3.9	14.6	435.1
3.8	14.7	429.7	3.4	14.4	368.9	4.1	14.7	463.6	4.1	13.9	414.5
3.7	15.9	489.5				4.3	14.2	453.7	4.2	14.1	436.9
3.5	14.7	395.8				4.5	12.1	344.7	4.5	13.8	448.4

									4.9	14.6	546.6
									5.9	12.7	498.1

Table S2. Quantification of chromatin folding demonstrates that CENP-C increases CENP-A chromatin clustering. Native chromatin incubated with or without the CENP-C fragment was visually inspected on AFM and identified as "open" or "clustered". Two independent analyses were performed (S2a and S2b). S2a: total number of CENP-A clusters per scan; S2b: total number of CENP-A clusters/total number of CENP-A nucleosome arrays per scan. Both analyses demonstrate that CENP-C increases CENP-A chromatin clustering (Methods).

Supplemental Table S2: Quantification of chromatin folding demonstrates that CENP-C increases CENP-A chromatin clustering

Supplemental Table S2a

Fig. S6B,C	ACA	ACA+CpC^{CD}	ACA WT	ACA CpC OE
Scan1	5	9	10	23
Scan2	9	5	11	14
Scan3	4	8	10	21
Scan4	4	6	9	22
Scan5	11	13	7	12
Scan6	11	12		
Scan7	5	12		
Scan8	5	11		

Supplemental Table S2b

Fig 3B,C	ACA WT			ACA CENP-C^{CD}		
	# arrays	# clusters	# cluster / # array	# arrays	# clusters	# cluster / # array
Scan1	14	5	0.36	19	7	0.37
Scan2	19	6	0.32	13	5	0.38
Scan3	22	6	0.27	14	6	0.43
Scan4	17	7	0.41	26	12	0.46
Scan5	34	13	0.38	15	6	0.40
Scan6	48	13	0.27	22	9	0.41
Scan7	40	16	0.40	24	11	0.46
	ACA WT			ACA CENP-C OE		
	# arrays	# clusters	# cluster / # array	# arrays	# clusters	# cluster / # array
Scan1	31	10	0.32	38	28	0.74
Scan2	34	11	0.32	50	27	0.54
Scan3	26	14	0.54	49	35	0.71
Scan4	19	7	0.37	55	39	0.71
Scan5	28	8	0.29	43	21	0.49

Table S3. RNAP2 levels on centromeric chromatin are reduced under CENP-C over-expression conditions
Cells were transfected (or not) with full length CENP-C which was over-expressed (OE) for 3 days, native centromeric chromatin was extracted by CENP-C or ACA ChIP, from wildtype cells or CENP-C OE cells, in parallel. Chromatin was evaluated for RNAP2 and CENP-A occupancy on Western blots. 3 indepedent replicates were quantified using the Licor scanner and automated software. Quantification of RNAP2 in CENP-C IP or ACA IP over Input demonstrates a suppression of RNAP2 levels on centromeric chromatin upon CENP-C OE, and a reduction of total CENP-A levels when RNAP2 is diminished.

Supplemental Table S3: RNAP2 levels are diminished upon centromeric chromatin in CENP-C over-expression conditions

RNAP2 quantification

	WT				CENP-C OE		
	Input	CENP-C IP	ACA IP		Input	CENP-C IP	ACA IP
Exp1	5.92	26.8	17.5	Exp1	6.52	9.12	8.76
Exp2	7.76	14.1	12.6	Exp2	9.36	7.5	10.8
Exp3	7.34	24.9	17.8	Exp3	6.31	8.07	7.67
		Ratio CpC/input	Ratio ACA/input			Ratio CpC/input	Ratio ACA/input
Exp1		4.53	2.96	Exp1		1.40	1.34
Exp2		1.82	1.62	Exp2		0.80	1.15
Exp3		3.39	2.43	Exp3		1.28	1.22
	mean	3.25	2.33		mean	1.16	1.24
	StDev	1.36	0.67		StDev	0.32	0.10

CENP-A quantification

	WT				CENP-C OE		
	Input	CENP-C IP	ACA IP		Input	CENP-C IP	ACA IP
Exp1	0.98	8.63	13.2	Exp1	1.97	6.74	8.53
Exp2	0.57	10	11.4	Exp2	0.56	8.7	2.18
Exp3	0.38	1.71	2.23	Exp3	0.52	1.6	2.02
		Ratio CpC/input	Ratio ACA/input			Ratio CpC/input	Ratio ACA/input
Exp1		8.81	13.47	Exp1		3.42	4.33
Exp2		17.54	20.00	Exp2		15.54	3.89
Exp3		4.50	5.87	Exp3		3.08	3.88
	mean	10.28	13.11		mean	7.34	4.04
	StDev	6.65	7.07		StDev	7.10	0.25

Table S4: CENP-C over-expression suppresses *de novo* CENP-A loading New CENP-A loading was distinguished from old CENP-A using TMR-Star followed by immunofluorescence (IF). Quantification of IF over 3 replicates demonstrates a 2.3 fold reduction in new CENP-A relative to old CENP-A on centromeres under CENP-C OE conditions relative to wildtype cells. Raw foci count are presented in Supplemental Raw Data File 2

Table S4: CENP-C over-expression suppresses de novo CENP-A loading			
TMR CENP-A foci/ Total CENP-A foci	WT	CENP-C OE	Fold-reduction of new (TMR) CENP-A
Mean TMR CENP-A/Total CENP-A foci	0.164	0.073	2.3
Standard deviation	0.082	0.042	
Standard error	0.008	0.004	
T-test (significance)			7.19384E-21